HHS Public Access

Author manuscript

Cell Host Microbe. Author manuscript; available in PMC 2021 June 10.

Published in final edited form as:

Cell Host Microbe. 2020 June 10; 27(6): 976–991.e11. doi:10.1016/j.chom.2020.03.025.

NON-NEUTRALIZING ANTIBODIES FROM A MARBURG INFECTION SURVIVOR MEDIATE PROTECTION BY FC-EFFECTOR FUNCTIONS AND ENHANCING EFFICACY OF OTHER ANTIBODIES

Philipp A. Ilinykh[1,3,*], **Kai Huang**[1,3,*], **Rodrigo I Santos**[1,3,*], **Pavlo Gilchuk**[4,*], **Bronwyn M. Gunn**[5,*], **Marcus M. Karim**[5], **Jenny Liang**[6], **Mallorie E. Fouch**[6], **Edgar Davidson**[6], **Diptiben V. Parekh**[7], **James B. Kimble**[1,3], **Colette A. Pietzsch**[1,3], **Michelle Meyer**[1,3], **Natalia A. Kuzmina**[1,3], **Larry Zeitlin**[8], **Erica Ollmann Saphire**[7,9], **Galit Alter**[5], **James E. Crowe Jr**[4,10,11,**], **Alexander Bukreyev**[1,2,3,12,**]

[1]Department of Pathology, University of Texas Medical Branch, Galveston, TX

[2]Department of Microbiology and Immunology, University of Texas Medical Branch, Galveston, TX

[3]Galveston National Laboratory, Galveston, TX

[4]Vanderbilt Vaccine Center, Vanderbilt University Medical Center, Nashville, TN

[5]Ragon Institute of MGH, MIT, and Harvard, Cambridge, MA

[6]Integral Molecular, Inc., Philadelphia, PA 19104, USA

[7]Department of Immunology and Microbiology, The Scripps Research Institute, La Jolla, CA

[8]Mapp Biopharmaceutical, San Diego, CA

[9]Skaggs Institute for Chemical Biology, The Scripps Research Institute, La Jolla, CA

[10]Department of Pathology, Microbiology, and Immunology, Vanderbilt University Medical Center, Nashville, TN

[11]Department of Pediatrics (Infectious Diseases), Vanderbilt University Medical Center, Nashville, TN

[**]Address correspondence to: Alexander Bukreyev, alexander.bukreyev@utmb.edu or James E. Crowe, Jr., james.crowe@vumc.org.
[*]These authors contributed equally.

AUTHOR CONTRIBUTIONS

P.A.I., K.H., R.I.S., P.G., J.E.C. and A.B. planned the studies. P.A.I., K.H., R.I.S., P.G., B.M.G., M.M.K., J.L., M.E.F., E.D., D.V.P., J.B.K., C.A.P., M.M. and N.A.K. conducted experiments. L.Z. provided antibodies. P.A.I., K.H., R.I.S., P.G., B.M.G., E.D., E.O.S., G.A., J.E.C. and A.B. interpreted the studies. P.A.I. and A.B. wrote the first draft of the paper. J.E.C. and A.B. obtained funding. All authors reviewed, edited, and approved the paper.

DECLARATION OF INTERESTS

P.A.I., J.E.C. and A.B. are listed as inventors on a submitted patent application, which covers antibodies described in the manuscript. J.E.C. has served as a consultant for Takeda Vaccines, Sanofi-Aventis U.S., Pfizer, and Novavax, is a member of the Scientific Advisory Boards of CompuVax and Meissa Vaccines and is Founder of IDBiologics. The Crowe laboratory at Vanderbilt University Medical Center has received sponsored research agreements from Moderna, Sanofi-Aventis U.S., and IDBiologics.

[12]Lead contact

Abstract

Marburg virus (MARV) and Ebola virus (EBOV) belong to the family *Filoviridae*. MARV causes severe disease in humans with high fatality. We previously isolated a large panel of monoclonal antibodies (mAbs) from B cells of a human survivor with previous naturally acquired MARV infection. Here, we characterized functional properties of these mAbs and identified non-neutralizing mAbs targeting the glycoprotein (GP) 2 portion of the mucin-like domain (MLD) of MARV GP, termed the wing region. One mAb targeting the GP2 wing, MR228, showed therapeutic protection in mice and guinea pigs infected with MARV. The protection was mediated by the Fc fragment functions of MR228. Binding of another GP2 wing-specific non-neutralizing mAb, MR235, to MARV GP increased accessibility of epitopes in the receptor-binding site (RBS) for neutralizing mAbs, resulting in enhanced virus neutralization by these mAbs. These findings highlight an important role for non-neutralizing mAbs during natural human MARV infection.

Graphical Abstract

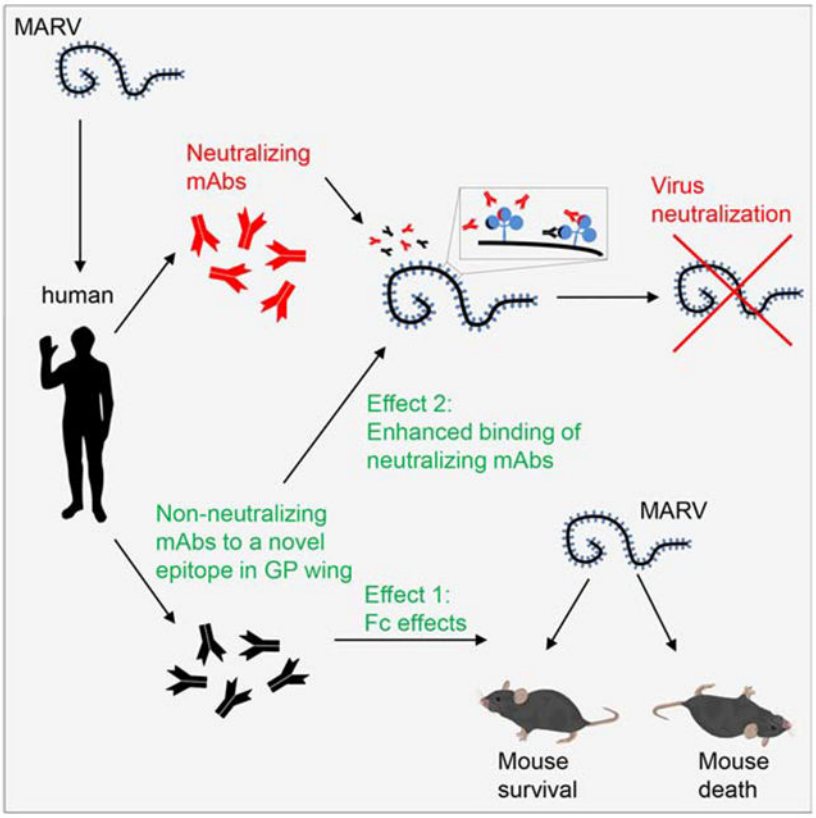

eTOC Blurb

Ilinykh et al. analyzed antibodies from a human survivor of Marburg virus infection and discovered biological properties for non-neutralizing antibodies that protect animals from lethal Marburg virus infection. These include inducing strong Fc domain-mediated effector functions and

structural glycoprotein rearrangements that facilitate access of neutralizing antibodies to their recognition sites.

INTRODUCTION

Filoviruses are enveloped, filamentous-like viruses with a non-segmented RNA genome of negative polarity, which comprise the *Marburgvirus* and *Ebolavirus* genera (Amarasinghe et al., 2017). *Marburgvirus* genus includes viruses Marburg (MARV) and Ravn (RAVV) while *Ebolavirus* genus includes viruses Ebola (EBOV), Sudan, Bundibugyo, Taï Forest, Reston and the recently discovered Bombali (Goldstein et al., 2018). Most of these viruses are known to cause severe disease with a high case fatality rate in humans. Previously, it was thought that filoviruses only cause local sporadic outbreaks in sub-Saharan Africa, but the unprecedented 2013-2016 EBOV epidemic in West Africa has changed this view (Burk et al., 2016; Holmes et al., 2016). The first known outbreak of MARV occurred in 1967 in Germany and Yugoslavia and was associated with the importation of rhesus macaques from Uganda (CDC, 2014; Malherbe and Strickland-Cholmley, 1968). The largest known outbreak of MARV occurred in 2004-2005 in Angola, which had a 90% case fatality rate (CDC, 2014; Towner et al., 2006).

Similarly to EBOV, virions of MARV are covered by the homotrimeric spikes of GP, the sole envelope viral protein responsible for cell entry. GP is a heavily glycosylated type I transmembrane protein, with O-linked glycans and many of the N-linked oligosaccharides clustered in the mucin-like domain (MLD) (Bukreyev et al., 1993; Feldmann et al., 1991; Will et al., 1993). The GP gene of ebolaviruses codes for the shorter secreted glycoprotein (sGP), while expression of the transmembrane full-length GP requires transcriptional editing of mRNA (Sanchez et al., 1996; Volchkov et al., 1995). In contrast, the GP gene of marburgviruses codes for transmembrane full-length GP; unlike ebolaviruses, marburgviruses do not produce sGP. GP undergoes trimerization within the endoplasmic reticulum; homotrimerization is essential for fusion activity of GP during viral entry into target cells (Mittler et al., 2013). In the trans-Golgi network, MARV GP is cleaved at the Arg-435 residue into GP1 (~160 KDa) and GP2 (~38 KDa) subunits. GP2 carries the transmembrane domain, is incorporated into the viral or cellular membrane, and is linked to GP1 via an intra-molecular disulfide bridge formed by the Cys-37 and Cys-610 residues (Mittler et al., 2013; Volchkov et al., 2000). During the lifecycle, all filoviruses share the requirement of proteolytic GP processing in endosomal compartments, which exposes the receptor-binding site (RBS) for the interaction with intracellular filovirus receptor, cholesterol transporter protein Niemann-Pick C1 protein (Carette et al., 2011; Cote et al., 2011), as a necessary step in cell entry. The cysteine endoproteases cathepsin B and cathepsin L were identified as key host enzymes that remove the MLD and glycan cap from filovirus GP (Chandran et al., 2005). It was shown for EBOV that these two domains shield RBS from access to the receptor in uncleaved GP (Lee et al., 2008). Although the use of endosomal cysteine proteases as host factors for entry is a general property of members of the family *Filoviridae*, it was shown with selective inhibitors that MARV, but not EBOV infection, is cathepsin B-independent, and that MARV might employ other cellular cysteine

or serine proteases in addition to or instead of cathepsins for cell entry (Gnirss et al., 2012; Misasi et al., 2012).

The recently published crystal structures of marburgvirus GP complexes with human mAbs obtained from a survivor of natural MARV infection (Flyak et al., 2015), MR78 (Hashiguchi et al., 2015) and MR191 (King et al., 2018), revealed certain differences in GP organization between ebolaviruses and marburgviruses. For example, the marburgvirus GP glycan cap is disordered and does not block antibody access to RBS effectively. The fact that the RBS is masked on the surface of EBOV (Lee et al., 2008), but is partially exposed on the surface of marburgviruses (Hashiguchi et al., 2015; King et al., 2018), may explain why RBS-targeting mAbs constitute the majority of known neutralizing antibodies elicited by marburgvirus described thus far (Flyak et al., 2015). Next, the marburgvirus MLD is larger than those of EBOV and projects less upward and covers the sides of the GP trimer. The equatorial projection of MLD, in addition to the absence of an ordered glycan cap, leaves the RBS more accessible in marburgviruses than in ebolaviruses (Hashiguchi et al., 2015; King et al., 2018). As a result of the furin cleavage site shift (Arg-435 in MARV and Arg-501 in EBOV), a part of MARV MLD, amino acids (aa) 436-501, stays attached to GP2 after proteolytic separation of GP precursor into subunits, whereas in EBOV the whole MLD lies within the GP1 subunit. This 66 aa-long part of MARV MLD, which remains associated with the GP2 subunit, termed the GP2 “wing”, is the only epitope other than the RBS that has been shown to elicit protective antibodies against marburgviruses (Fusco et al., 2015).

There are no licensed therapeutics available against the disease caused by filoviruses. Antibodies currently represent the most promising platform for the development of pre- or post-exposure prophylactic or therapeutic treatments of filovirus-induced disease and are critical tools for design of improved vaccines. Currently mAb-based products are being evaluated in Ebola virus disease (EVD) patients in the ongoing outbreak in the Democratic Republic of the Congo. Human mAbs are characterized by a relatively long half-life, a low rate of adverse reactions, are amenable to mass production, and provide immediate antiviral protection (Wong et al., 2014). The 2013-2016 epidemic of EBOV resulted in quick progress in development and clinical testing of multiple antibodies and vaccines against this virus, while similar studies with MARV lag behind. One of the human mAbs that we previously isolated from the blood of a MARV infection survivor (Flyak et al., 2015), the anti-RBS mAb MR191, is the only antibody demonstrated so far to confer complete NHP protection when given as late as 5 days after virus challenge (Mire et al., 2017). Although MR191 viral escape mutants have not been observed *in vivo,* they can be generated *in vitro* (Flyak et al., 2015; King et al., 2018), raising a hypothetical concern about its use as a monotherapy. Here, we present a comprehensive study of biological properties of a panel of MARV mAbs from a human survivor (Flyak et al., 2015). We found that the non-neutralizing mAbs MR228 and MR235 strongly mediated neutrophil and monocyte phagocytosis and natural killer (NK) cell activation, with MR228 conferring *in vivo* protection through the induction of Fc domain-mediated mechanisms. We also show that MR228 and MR235 possess overlapping epitopes in the GP2 wing region. Next, we show that interaction of MR235 mAb with GP exposes neutralizing epitope(s) and dramatically increases binding of RBS-specific mAbs to membrane-anchored GP, which results in enhanced virus neutralization. These data suggest a cooperative mechanism for MARV neutralization by antibodies that

target different GP epitopes and an important role of non-neutralizing mAbs in virus clearance during infection.

RESULTS

Most of the tested neutralizing mAbs and a single non-neutralizing MR228 mAb protect against MARV challenge *in vivo*

In previous work, we isolated and characterized multiple mAbs from the blood of a human survivor of natural MARV infection (Flyak et al., 2015). Here, we selected representative mAbs from the four noncompeting groups, based on kinetics of their binding to full-length and mucin-deleted (GPΔmuc) ectodomains of MARV GP: three mAbs from group 1 (bind GPΔmuc better than full-length GP), two mAbs from group 2 (bind full-length GP better than GPΔmuc), three mAbs from group 3A and 19 mAbs from group 3B (group 3 mAbs bind both full-length GP and GPΔmuc, with group 3B antibodies possessing lower K_D of GP binding) (Flyak et al., 2015), most of which belong to the IgG1 subclass (Fig. 1). We performed broad characterization of the panel including testing of their protective efficacy and Fc fragment-mediated effector functions (Fig. 1, 2, S1–S3), and one additional mAb from group 3A, MR224, was tested for protective efficacy only. All 28 mAbs were tested initially using the conventional mouse lethal challenge model for MARV. Animals were exposed to 1,000 plaque-forming units (PFU) of mouse-adapted MARV strain Ci67 (Warfield et al., 2007) and 24 h later administered 100 μg (approximately 5 mg/kg) of MARV mAbs or the irrelevant mAb 2D22 specific for dengue virus serotype II (Fibriansah et al., 2015) by the intraperitoneal route (Fig. S1). Sixteen antibodies were found to confer 80 to 100% protection from the otherwise lethal dose of MARV, with all except one mAb (MR228) belonging to group 3B (RBS-specific), which includes all neutralizing mAbs in the panel.

Wing-specific antibodies induce strong Fc-mediated effects

To assess Fc fragment-mediated effector functions, we analyzed antibody-dependent neutrophil phagocytosis (ADNP), antibody-dependent monocyte phagocytosis (ADCP) and activation of NK cells (Fig. 1, 2, S2, S3) using methodologies developed and tested in our previous studies (Gunn et al., 2018; King et al., 2018). To analyze induction of phagocytosis, mAbs were added to MARV GP-coated fluorescent beads and incubated with white blood cells from human donors or THP-1 monocytes; FITC-positive neutrophils or monocytes were analyzed by flow cytometry. For the NK cell activation assay, mAbs were added to MARV GP coated onto 96-well plates, and then human NK cells were added and analyzed for the activation markers CD107a, IFNγ and MIP-1β by flow cytometry. The levels of the marker of degranulation of CD107a and intracellular cytokines IFNγ and MIP-1β are typically used to describe the activation status of NK cells (Alter et al., 2004). Interestingly, the highest levels of phagocytosis (Fig. 2A, S2A,B, S3A,B) and activation of NK cells (Fig. 2B, S2C–E, S3C) were observed for two non-neutralizing mAbs: MR228 and MR235 from group 2; high phagocytosis was also induced by the non-neutralizing MR221 mAb from group 3A. For MR221, however, this finding can be explained by its belonging to the IgG3 subclass, which has a higher affinity for the activating Fcγ-receptors (FcγR) over the other IgG subclasses (Bruhns et al., 2009). Remarkably, unlike MR228 and MR235, MR221 failed

to activate NK cells. The Fc-mediated effects of MR228 and MR235 were further validated with MARV-infected Vero-E6 cells, which further confirmed the strong induction of ADNP and ADCP (Fig. 2C, S3D,E). Taken together, these results demonstrate that mAbs targeting the wing region of MARV GP mediate a high level of Fc domain-mediated activity.

MR228 and MR235 mAbs bind to epitopes located in GP2 wing

To determine if the MR228 and MR235 epitopes are linear or conformational, we assessed interaction of mAbs with MARV and RAVV GPs in non-reducing versus reducing conditions by western blot (Fig. S4A). MR228 recognized GP2 of MARV strains Musoke and Angola equally well regardless of the conditions, but only heat-denatured DTT-reduced form of RAVV GP2. These data correspond to the strong MR228 binding to MARV GP2 and its weak binding to RAVV GP2 (Fig. 1). We also observed a very weak binding of both mAbs to GP1. The enhancement of binding to heat-denatured reduced RAVV GP over the folded protein suggests that the epitope for MR228 is linear. Consistent with the potent MR235 binding to GPs of all marburgviruses tested (Fig. 1), heat denaturation and reduction of MARV and RAVV GPs did not affect their recognition by MR235, suggesting that its epitope is also linear (Fig. S4A).

We next sought to determine the epitopes of MR228 and MR235. First, we attempted to generate escape mutants by performing eight consecutive passages of the recombinant vesicular stomatitis virus in which the envelope G protein is replaced with GP of MARV 200702854 Uganda (VSV/MARV-GP), previously developed in our laboratory (Flyak et al., 2015) in the presence of increasing concentrations of MR228. Sequencing of GP ORF from the last virus passage did not identify any mutations compared to the input virus used for the first passage, which was not unexpected given that MR228 mAb is non-neutralizing.

To identify MR228 and MR235 epitopes, we generated a series of 18 MARV GP plasmid constructs bearing deletions or alanine substitutions in different parts of GP (Fig. 3A, S4B, Table S1). The panel included mutations in GP domains previously identified as epitopes for MARV-specific mAbs, such as the glycan cap and MLD (Flyak et al., 2015; Fusco et al., 2015; Kajihara et al., 2013), and in the IFL and MPER, since corresponding regions of EBOV GP2 subunit were also found to be immunogenic (Flyak et al., 2018; Flyak et al., 2016; Ilinykh et al., 2018b; Kuzmina et al., 2018). The constructs were surface-expressed in 293T cells by transient transfection, then primary anti-MARV antibodies were added, followed by fluorescently labeled secondary antibodies, and flow cytometric analysis of cell populations was performed. Two rabbit polyclonal sera were used as control reagents to detect the expression of GP mutants. In addition, binding of MR186 from another competition-binding group, which targets the RBS (Flyak et al., 2015), was evaluated for comparative purposes. Both polyclonal sera and the RBS-binding mAb MR186 bound well to wild-type GP, demonstrating robust GP display on the surface of transfected cells (data not shown). Compared to wild-type GP, binding of MR228 to mutated GP constructs #1 (D449A/N453A/D457A/D459A), #2 (450GLIN453 → AAAA), #9 (Del 451-471 aa) and #12 (Del 441-459 aa) was substantially impaired. At the same time, deletion of the C-terminus of GP1 and the N-terminus of GP2 (construct #10), or deletion of the whole GP2 wing region (construct #11) both resulted in a dramatic reduction of binding or the complete

lack of binding to all tested polyclonal and monoclonal antibodies, possibly due to altered GP conformation. In contrast, none of the single mutations introduced in the 597-608 aa region caused an impairment of GP interaction with MR228, MR235, or control rabbit antisera (Table S1, Fig. 3A; binding data are shown only for the W598A mutant, Fig. S4B). Reduction in binding by MR235 was only observed with the amino acid deletion 441-459 (construct #12), together with MR228, indicating this region likely includes part(s) of the epitope shared by the two antibodies. However, mutations introduced in constructs #1 and #2 did not affect MR235 binding, but were critical for MR228 binding, confirming that these mAbs occupy overlapping, but not identical epitopes in the GP2 wing region. The epitopes for MR228 and MR235 were mapped further by alanine scanning of MARV GP, transient expression in transfected 293T cells and analysis of binding to the mAbs by flow cytometry as in our previous studies (Flyak et al., 2016, 2018; Gilchuk et al., 2018). The analysis demonstrated diminished binding (in most cases <20% of binding to wild-type MARV GP) of the mutants P446A, F447A, I452A and N453A for MR228 and the mutants W439A, F445A, P446A and F447A for MR235, but a high level of binding by these mutants to the control mAb MR78 (Flyak et al., 2015). The mutations were modeled with MARV GP structure (PDB id 6BP2) (King et al., 2018) (Fig. S4C).

At the same time, mAb binding in a peptide microarray revealed two overlapping areas of GP as possible contact sites for MR228 (Fig. 3B) and MR235 (Fig. 3C). The MR228 binding peak corresponded to three overlapping 15-mer peptides spanning amino acids 441-463 of GP, with the highest median fluorescence intensity observed for peptide #112 (445-459 aa), followed by peptides #111 (441-455 aa) and #113 (449-463 aa). The MR235 binding peak corresponded to two peptides spanning amino acids 437-455, with the highest signal raised by antibody binding to peptide #110 (437-451 aa), followed by peptide #111. The region from 437 to 463 aa lies within the wing domain, which was demonstrated to be an epitope for protective murine mAbs raised by immunization with RAVV GPΔmuc antigen (Fusco et al., 2015). These mAbs possess only moderate neutralizing activity against the GP pseudotyped VSV construct; neutralization of the authentic RAVV was not tested (Fusco et al., 2015). To determine whether MR228 and MR235 share epitopes with published murine antibodies targeting the GP2 wing (Fusco et al., 2015), a competition-binding assay with full-length MARV GP expressed on the surface of stably transfected Jurkat cells was performed (Fig. 3D). Curiously, competition was not detected between MR228 and 30G4 or between MR235 and 30G4, despite the proximity of epitopes on the linear GP structure. In fact, binding of 30G4 was increased in the presence of MR235. These data suggest the presence of at least two non-overlapping antibody epitopes within the wing region. Altogether, these data indicate that the *in vivo* protective, non-neutralizing MR228 binds a linear epitope within the GP2 wing region, which partially overlaps with that of the GP2 wing murine mAb 30G4 (Fig. 3E). The MR235 epitope also partially overlaps with the epitope of MR228 but shifts slightly toward the furin cleavage site and does not overlap with that of 30G4. Taken together, these data suggest that the non-neutralizing, but protective mAb MR228 and mAb MR235 bind to epitopes located in the GP2 wing region, and possibly weakly interact with GP1.

Protection by the non-neutralizing antibody MR228 is mediated by Fc fragment effector functions

We next asked if the single non-neutralizing mAb identified in the study that protects *in vivo*, MR228, confers protection of infected animals through the engagement of FcγRs at the surface of effector immune cells, or activation of complement-dependent cytotoxicity. For that, we produced two recombinant mutated versions of this antibody: one bearing the mutations L234A/L235A in the Fc fragment (rMR228-LALA), which impairs antibody binding to FcγRs, and another variant antibody with the mutation K322A (rMR228-KA) which greatly reduces binding to human complement C1q resulting in the lack of efficient activation of human complement (Hessell et al., 2007; Hezareh et al., 2001). Comparison of the protective efficacy of the mutated mAbs with the recombinant non-mutated MR228 in mice demonstrated that the LALA mutation abolished protection, whereas the KA mutation did not (Fig. 4A). These results suggest that engagement of FcγRs by innate immune cells (Fig. 1, 2, S2, S3), but not activation of the complement system, is required for *in vivo* protection by MR228 mAb in the mouse model of MARV infection.

To compare the protective efficacy of wild-type or LALA-bearing MR228 in a more stringent model, we inoculated guinea pigs with 1,000 PFU of guinea pig-adapted MARV (Shedlock et al., 2013) and 24 h later administered a single 5 mg antibody dose (approximately 10 mg/kg) (Fig. 4B). In both rMR228 and rMR228-LALA groups, two out of five animals (40%) survived in the mAb-treated group, whereas all animals in the control group succumbed to infection on days 8-10.

We next asked if the protection observed by MR228 in mice and guinea pigs is conferred through a reduction in virus titers. To address this question, we inoculated mice with MARV, 24 h later treated with rMR228, rMR228-LALA, the neutralizing mAb MR191N or the irrelevant mAb 2D22, and on day 5 post-infection collected mesenteric lymph nodes, liver, spleen and serum. Virus load was quantified by plaque assay or analysis of virus-infected cells by flow cytometry (Fig. S5A–D). As expected, MR191N strongly reduced virus replication in all tissues analyzed. Despite the lack of the neutralizing activity, rMR228 also strongly reduced MARV titers in spleen, marginally reduced in blood, and strongly reduced the numbers of virus-positive cells in lymph nodes, while the LALA mutation reversed these effects to various degrees. Plaque titration of MARV in blood of guinea pigs treated with rMR228 or rMR228-LALA (Fig. 4B) demonstrated that similarly to mice, rMR228 did significantly reduce viral titers, while the LALA mutation partially abrogated this effect (Fig. S5E).

As dendritic cells and cells derived from monocyte-macrophage lineages are among the primary targets of EBOV infection *in vivo* (Baize et al., 2000; Geisbert et al., 2003), we performed confocal microscopic analysis of lymph nodes from infected mice treated with mAbs to better understand the mechanisms of protection by MR228. Mice were inoculated with MARV or phosphate buffered saline (PBS) on day 0, treated with mAbs on day 1 and euthanized on days 2 or 5. The previously characterized neutralizing RBS-specific MR191 mAb (Flyak et al., 2015; King et al., 2018) was included for comparative purposes. We combined MARV staining with staining specific for neutrophils (Ly6G), NK cells (NK1.1), macrophages (F4/80) or lymphocytes (CD3) (Fig. 5, S6). MARV infection resulted in the

appearance of virus-positive cells in lymph nodes, which increased by day 5 post-infection (Fig. 5A, S6A). We also observed an influx of neutrophils (Fig. 5A, left panel), which was especially strong on day 5, and an influx of NK cells (Fig. S6A, left panel) and macrophages (Fig. 5A, right panel) at both time points. In contrast, the numbers of T cells in lymph nodes were reduced, especially on day 5, when almost no T cells were observed (Fig. S6A, right panel). Antibody treatments reversed the depletion of T cells induced by the infection. Interestingly, introduction of the LALA mutation in MR228 changed the pattern of migration for neutrophils (Fig. 5A, left panel) and NK cells (Fig. S6A, left panel); however, the LALA mutation did not affect the recovery of T cells observed with the non-mutated antibody (Fig. S6A, right panel). These findings were further confirmed for macrophages by flow cytometry analysis of mesenteric lymph node cells, which demonstrated a significant influx of the cells in rMR228-treated animals, as compared to MR191N-treated animals (Fig. 5B). Taken together, these data suggest that the protection observed in MR228 treated animals is, at least in part, conferred through Fc-mediated effects, which reduce viral titers in blood and tissues.

The non-neutralizing antibody MR235 increases binding of neutralizing mAbs resulting in enhanced virus neutralization

Some combinations of mAbs can substantially reduce dosage of individual components due to their cooperative effect on viral inhibition (Howell et al., 2017). Moreover, given the possibility of virus escape from antibody pressure through accumulation of mutations in the targeted protein, mixtures of antibodies with different epitope specificities may be preferable to a single potent neutralizing antibody monotherapy. We sought to test whether non-neutralizing mAbs from our panel could act cooperatively with neutralizing mAbs. MARV neutralization by combinations of mAbs was compared with the individual mAb components in each combination (Fig. 6, S7). The concentration of each mAb used in combination was two times lower than the concentration of neutralizing or non-neutralizing mAbs used alone. Therefore, the total dose of antibody was equal. When tested along with group 3B neutralizing antibodies, MR235 significantly increased the overall virus neutralization potency in a dose-dependent manner. This effect was observed regardless of the presence or absence of complement in the medium. The cooperative effect was not limited to any specific mAb; all tested neutralizing mAbs demonstrated clear cooperation in combination with MR235. The 50% maximal inhibitory concentrations (IC_{50}) of antibody cocktails were significantly lower than those of any individual antibody. In comparison, the addition of MR228, which similarly to MR235 belongs to group 2 (Fig. 1), did not demonstrate consistent effects when combined with neutralizing mAbs (Fig. 6). Presumably, since the MR235 epitope spans more distal toward the N-terminus of the wing domain (Fig. S4C), it is easier for this mAb rather than MR228 to displace the GP2 wing on a lever mode, thus exposing the RBS and making it accessible for neutralizing mAbs.

We hypothesized that the observed neutralization cooperation is mediated by enhanced binding of neutralizing antibodies to MARV GP in the presence of MR235. To test this hypothesis, we used a cell-surface display system with Jurkat cells expressing MARV GP (Bramble et al., 2018; Davis et al., 2019). Corresponding to our previous data on binding of mAbs to plate-adsorbed soluble recombinant GP antigen (Flyak et al., 2015), we found that

binding of neutralizing mAbs MR78 and MR191 to MARV GP expressed on the cell surface was not as strong as that of MR228 or MR235 (Fig. 7A), suggesting their epitopes are partially shielded from immune recognition in the membrane-associated form of GP. In contrast, the epitopes for MR228 and especially MR235 were easily accessible, as evidenced by saturable binding of these mAbs to GP-expressing cells. When labeled MR78 or MR191 antibodies were added to cells in the presence of a saturating concentration of unlabeled MR235, their ability to bind to the native conformation of MARV GP increased significantly (Fig. 7B). These data suggest the indispensable role of antibody cooperation during natural filoviral infection, as binding of non-neutralizing antibodies can change GP conformation and expose otherwise hidden epitopes, facilitating access by neutralizing antibodies. It should be noted that these mAbs were isolated from a single individual who survived MARV disease.

To confirm that certain epitopes may be shielded from antibody access in the natural GP conformation, we assessed mAb binding to the surface-expressed MARV GP upon brief proteolytic priming with thermolysin which generates cleaved GP (GP_{CL}). This bacterial metalloproteinase mimics the proteolytic processing of filovirus GPs by cathepsins B/L inside endosomal compartments of the host cell (Chandran et al., 2005; Dube et al., 2009; Schornberg et al., 2006). Brief proteolytic priming of MARV GP exposed at the cell surface resulted in a rapid exposure of the epitopes occupied by group 3B mAbs MR78, MR191 and MR65 (Fig. 7C). These results are similar to previous findings with EBOV GP showing that cleavage with thermolysin removes the glycan cap and exposes the RBS (Bornholdt et al., 2016). Unlike for EBOV GP, the longer digestion of MARV GP by thermolysin did not result in any further exposure of epitopes to neutralizing mAbs, but instead led to a decline of binding, presumably due to a gradual proteolytic degradation of the epitopes (data not shown). In contrast, the epitopes of group 2 mAbs MR228 and MR235, as well as the murine mAb 30G4, degraded shortly after thermolysin treatment (Fig. 7C), suggesting that in addition to the better recognition of the wing epitope by mAbs (Fig. 7A), this epitope is also more sensitive to proteolytic degradation.

We next performed profiling of the survivor's plasma by testing plasma Abs binding to intact and cleaved Jurkat-MARV GP. Interestingly, plasma Ab binding was ~270-fold higher to thermolysin-cleaved GP than to intact GP (Fig. 7D), suggesting that most of the plasma MARV-neutralizing activity is mediated by RBS-specific mAbs or the other mAb specificities that recognize proteolytically cleaved GP. This finding is similar to the recent report for plasma Abs of EVD survivors that preferentially targeted the cleaved form of EBOV GP (Davis et al., 2019). To investigate further the prevalence of anti-wing and anti-RBS mAbs in the survivor's plasma, we performed a competition-binding assay with human mAbs of known epitope specificity using intact (two anti-wing mAbs) or cleaved (two anti-RBS mAbs) cell surface displayed MARV GP. Cells were pre-incubated with dilutions of plasma from the survivor or a control donor and then stained with respective fluorophore-labeled human mAbs. At the lowest plasma dilution tested (1:50), polyclonal plasma Abs fully inhibited binding of MR78 or MR191, while at the highest plasma dilution tested (1:1,350), the reduction in both mAbs binding by ~84% was observed. The control non-immune plasma did not exhibit any detectable blocking activity for anti-RBS mAbs (Fig. 7E). In contrast, competition binding was not detected for anti-wing mAbs. These data

suggest the high prevalence of anti-RBS Abs and low frequency of anti-wing mAbs in the immune repertoire of the MARV survivor, which is consistent with our previous mAb work (Flyak et al., 2016). Taken together, these data demonstrate that rare non-neutralizing antibodies specific to the N-terminus of the GP wing domain can change GP conformation resulting in enhanced access of neutralizing mAbs to RBS and increased virus neutralization.

DISCUSSION

Here, we present the results of in-depth biological characterization of the panel of MARV mAbs previously isolated from the blood of a survivor of MARV disease (Flyak et al., 2015). Two antibodies representing the same binding group, MR228 and MR235, revealed unique biological properties of strong binding to marburgvirus GPs and induction of multiple Fc-effector protective mechanisms, accompanied by the complete lack of virus neutralizing activity (Fig. 1, 2, S1–S3). Nevertheless, mAb MR228 conferred complete (100% survival) protection in mice (Fig. 1, 4A, S1) and partial protection (40% survival) in guinea pigs (Fig. 4B) from the otherwise uniformly lethal MARV infection. Using complementary approaches, MARV GP mutagenesis, including alanine scanning (Fig. 3A, S4B,C) and peptide binding assays (Fig. 3B,C), we localized the epitopes for MR228 and MR235 to the N-terminus of the wing domain located in the GP2 subunit (Fig. 3E). However, MR228 and MR235 did not compete with another wing-specific mAb described previously, the murine mAb 30G4 (Fusco et al., 2015), for binding to cell surface-expressed MARV GP (Fig. 3D). Notably, mAb 30G4 was raised by immunization of mice with an artificial RAVV GPΔmuc construct lacking most of the GP1 portion of MLD (257-425 aa), which comprises ~70% of the whole MLD, while MR228 and MR235 represent products of the human B cell response to MARV infection. This difference may explain the different characteristics of mAb binding to plate-adsorbed purified proteins: 30G4 better interacts with GPΔmuc (Del 257-425 aa) than with full-length GP (Fusco et al., 2015), while MR228 binds to GPΔmuc (Del 257-425 aa) less efficiently than to full-length GP, and MR235 does not bind to GPΔmuc at all (Flyak et al., 2015). The kinetics of MR228 and MR235 binding to thermolysin-cleaved GP (Fig. 7C) demonstrate that their epitopes likely are disturbed during the proteolytic processing of viral GP inside endosomes (Gnirss et al., 2012; Misasi et al., 2012). Although the epitopes of MR228 and MR235, which are linear, are located close to each other, or even overlap (Fig. 3E), it is possible that in our cell surface display assay, binding of a primary mAb changes GP conformation and exposes additional point(s) of contact on the GP molecule, which can be occupied by a second mAb, along with the accessible main part of the epitope. For MR228 and MR235, such additional point(s) of contact may be located somewhere in the GP1 portion of MLD (Flyak et al., 2015). Neither MR228 nor MR235 competed for binding with the known wing mAb 30G4, which cross-reacts with three strains of MARV (Angola, Musoke and Ci67) (Fusco et al., 2015), for binding to MARV strain Angola. Furthermore, MR228 and MR235 are unlikely to induce selection of escape MARV mutants because they do not neutralize and because the wing domain is much more conserved than MLD (Fig. S8) and therefore is less likely to tolerate mutations.

Since MR228 was the only non-neutralizing mAb identified to completely protect mice in our study, we sought to determine whether this protection was mediated by engagement of Fc-effector mechanisms. Indeed, the version of MR228 which contains mutations in its Fc fragment abrogating interaction with FcγRs, rMR228-LALA, completely lost the ability to protect mice from MARV infection (Fig. 4A). The rMR228-mediated protection was accompanied by reduced viral load in spleen and lymph nodes; the effect was partially abrogated by the LALA mutation (Fig. S5A,D). In guinea pigs, the LALA mutation did not affect survival (Fig. 4B) but did partially reverse the reduction of viremia by the mAb (Fig. S5E). Several mutations in various parts of the Fc domain are known to affect its Fc-mediated protective effects: L234A and L235A (Jacobsen et al., 2017) and N297Q in the lower hinge impair binding to FcγRs (Wines et al., 2000), K322A in the N-terminus of the CH2 domain reduces binding to C1q (Hezareh et al., 2001); many other mutations have various biological effects (Crowe et al., unpublished data). It is possible that the former mutation used in our study does not abrogate the Fc-mediated protective effects in guinea pigs as fully as in mice. Another possibility is that, in addition to its ability to induce strong Fc-mediated effects, MR228 can also suppress viral infection through the Fab domain, as it was previously shown that MLD-specific non-neutralizing mAbs can inhibit MARV replication by abrogation of virion budding from infected cells (Kajihara et al., 2012). Thus, protection by MR228 *in vivo* may result from both Fc- and yet to be defined Fab-activities. In the guinea pig model of infection, an Fc-mediated MR228 functions may, therefore, be less critical for animal survival compared to the mouse model of MARV infection.

We found that both non-neutralizing mAbs, MR228 and MR235, induced strong phagocytosis of immune complexes by neutrophils and monocytes and activation of NK cells (Fig. 1, 2, S2, S3). Supporting these *in vitro* data, the immunofluorescence analysis of lymph nodes from infected animals indicated that rMR228-treated animals presented neutrophils (Fig. 5A, left panel) and NK cells (Fig. S6A, left panel) found as dense groups, very frequently around infected cells, in contrast to lymph nodes from mock-treated animals in which these cells were unresponsive to infected cells. Neutrophils in lymph nodes of mice treated with rMR228-LALA were spread diffusely, similarly to mock-treated infected animals, consistent with the role of Fc-mediated effects in protection mediated by this mAb. Moreover, the absence of CD3 staining in mock-treated infected animals and the presence of CD3-positive cells in animals treated with either rMR228 or rMR228-LALA (Fig. S6A, right panel) also were consistent with the *in vivo* protection data.

While MR228 and MR235 belong to the IgG1 subclass, as most of the other mAbs in the panel (Fig. 1), they comprise a separate competition-binding group (Flyak et al., 2015). This finding suggests that the ability of MR228 and MR235 to activate Fc effector mechanisms depends on their epitope specificities, rather than the structural organization of Fc fragments. The link between epitope localization and the efficiency of activation of Fc-related immune mechanisms has been recently demonstrated for antibodies specific to influenza virus (Henry Dunand et al., 2016; Leon et al., 2016; Mullarkey et al., 2016). Besides Fc-FcγR interaction, such activation requires binding of influenza virus hemagglutinin (HA) to the sialic acid (SA) receptor at the surface of an effector cell, explaining why stalk-specific antibodies, but not antibodies interfering with the SA-binding site in the HA head domain, appear more likely to induce antibody-dependent cellular cytotoxicity (Leon et al., 2016).

The RBS of MARV is more accessible for antibodies compared to that of EBOV (Hashiguchi et al., 2015; King et al., 2018). An equivalent region of the EBOV GP base in MARV is likely shielded by the GP2 wing domain (King et al., 2018), which is further supported by the fact that the RBS and the wing region are still the only two protective epitopes identified for MARV antibodies (Flyak et al., 2015; Fusco et al., 2015), with no protective mAbs recognizing the MARV GP base or MPER reported to date. The effect we have found here for MR235 and RBS-targeting mAbs resembles the cooperation shown for EBOV mAbs (Howell et al., 2017). In our experimental system, binding of neutralizing mAbs to MARV GP expressed at the surface of Jurkat cells was weaker than that of MR228 or MR235, and addition of MR235 mAb led to a substantial increase in GP binding by neutralizing antibodies (Fig. 7A,B). Interestingly, however, virus neutralization *in vitro* by MR191 and MR78 mAbs does not require presence of additional mAbs (Flyak et al., 2015), suggesting that in cell surface display, RBS epitopes can be occluded due to stoichiometry factors, such as density of GP spikes, their angle to the membrane, or some lipid/protein structural components of the plasma membrane. Nevertheless, the results of the binding assay (Fig. 7A,B) and virus neutralization *in vitro* (Fig. 6) clearly indicate that the MR235 mAb has the potential to strongly enhance the antiviral activity of neutralizing mAbs that recognize RBS epitopes. As MR235 enhanced neutralization of four different neutralizing mAbs tested, it is likely to enhance protection during natural infections which induce polyclonal antibody response. Short-term proteolytic cleavage of MARV GP with thermolysin releases RBS epitopes by removing the epitopes normally occupied by wing mAbs in full-length GP (Fig. 7C). The cooperative mechanism observed for MR235 may therefore functionally mimic the action of proteases: relocation of MLD resulting in RBS exposure. Moreover, MR235 not only uncovered GP for efficient recognition by RBS mAbs, but also increased binding of the wing-specific mAb 30G4 (Fig. 3D), which is partially neutralizing and protective *in vivo* (Fusco et al., 2015). The location of MR235 epitope proximal to the furin cleavage site (*i.e.*, at the GP1/GP2 border; Fig. 3E) probably leads to the critical change of GP conformation upon MR235 binding, allowing access for other mAbs with diverse epitopes to otherwise hidden GP areas. Overall, these data suggest an important cooperative role for non-neutralizing mAbs like MR235 in the context of natural MARV infections as cofactors for other mAbs with diverse epitopes, potentiating or enforcing their biological activity.

In summary, we discovered unique biological properties for human mAbs targeting the wing domain of MARV glycoprotein and their role in protection against natural MARV infection: recruitment of immune cells via Fc-FcγR interactions for the rapid clearance of infection, and structural GP rearrangements upon binding, which result in RBS exposure and facilitate an access of neutralizing mAbs to their recognition sites on the GP molecule. Moreover, given the relative conservation of the N-terminal part of the GP2 wing region among marburgviruses (Fig. S8) and the fact that these mAbs are non-neutralizing and therefore, are unlikely to induce virus escape mutants, these properties make them attractive candidates for therapeutic mAb-based cocktails against MARV infection.

STAR METHODS

LEAD CONTACT AND MATERIALS AVAILABILITY

Further information and requests for reagents may be directed to, and will be fulfilled by, the lead contact Alexander Bukreyev (alexander.bukreyev@utmb.edu). All unique/stable reagents generated in this study are available from the Lead Contact upon request.

EXPERIMENTAL MODEL AND SUBJECT DETAILS

Cell lines.—Vero-E6 (monkey, female origin), THP-1 (human, male origin), and HEK-293T (human, female origin) cell lines were obtained from the American Type Culture Collection (ATCC). Vero-E6 cells were cultured in Minimal Essential Medium (MEM) (ThermoFisher Scientific) supplemented with 10% fetal bovine serum (FBS; HyClone) and 1% penicillin-streptomycin (ThermoFisher Scientific) at 5% CO_2, 37°C. THP-1 cells were cultured in RPMI 1640 medium (Sigma-Aldrich) supplemented with 10% heat-inactivated FBS (Sigma-Aldrich), 100 units/mL of penicillin, and 100 μg/mL of streptomycin (Gibco), and 55 μM beta-mercaptoethanol (Gibco) at 37°C in 5% CO_2. HEK-293T cells were cultured in Dulbecco's Modified Eagle's Medium (ThermoFisher Scientific) with 10% heat-inactivated FBS, 2mM L-glutamine and 1% penicillin-streptomycin (ThermoFisher Scientific). ExpiCHO (hamster, female origin), Expi293F (human, female origin) and FreeStyle 293F (human, female origin) cell lines were purchased from ThermoFisher Scientific and cultured according to the manufacturer's protocol. Jurkat-MARV GP (strain Angola2005, GenBank: DQ447653) similar to previously reported Jurkat-EBOV GP (Davis et al., 2019) and untransduced Jurkat cells (human, male origin) were provided by Drs. Rafi Ahmed and Carl W. Davis (Emory University).

Viruses.—MARV strain 200501379 Angola (MARV-Angola) was isolated during the outbreak in Angola in 2005 (Towner et al., 2006) and passaged three times in Vero-E6 cells. The mouse-adapted Ci67 strain of MARV (Warfield et al., 2007) used in all experiments with mice was provided by Dr. S. Bavari (USAMRIID) and amplified by a single passage in Vero-E6 cells. The guinea pig-adapted Angola strain of MARV used for infection of guinea pigs was provided by Dr. G. Kobinger (while at the Canadian National Microbiology Laboratory). This virus was isolated originally from a patient in Angola, passaged once in Vero-E6 cells, passaged eight times in Hartley guinea pigs using liver and spleen homogenates, once in Vero PP cells, and once in Vero cells for stock production. All work with MARV was performed in the BSL-4 and ABSL-4 facilities in the Galveston National Laboratory. The chimeric eGFP-expressing EBOV/MARV-GP virus was used to test mAb combinations in neutralization assay in HTS format (Ilinykh et al., 2016). The construction of VSV/MARV-GP virus was described elsewhere (Flyak et al., 2015).

Antibodies.—Generation of hybridoma-produced mAbs obtained from a human survivor of a natural MARV infection is described elsewhere (Flyak et al., 2015). In some of the experiments, recombinant mAbs were used which were produced in mammalian Expi293F cells: rMR228 in Fig. 2C, 4, 5, S3D,E, S5, S6; rMR228-LALA in Fig. 2C, 4, 5, S3D,E, S5, S6A; rMR228-KA in Fig. 4A; or in tobacco (*Nicotians benthamiana*) plants: MR186N in

Fig. 3A and MR191N in Fig. 5, 6, S1, S5A–D, S6, S7. The tobacco-derived mAbs were generated as previously described (Zeitlin et al., 2011).

***In vivo* experiments.—**The animal experiments were performed in accordance with NIH guidelines, the Animal Welfare Act, and US federal law and approved by the Institutional Animal Care and Use Committee. Prior to experimentation, animals were given at least one week to acclimatize to the Galveston National Laboratory ABSL-4 facility. Seven-week-old BALB/c female mice (The Jackson Laboratory) or 5- to 6-week-old female guinea pigs (strain Hartley, Charles River Laboratories) were placed in the ABSL-4 facility in the Galveston National Laboratory. Groups of five animals were injected intraperitoneally with 1,000 PFU of the mouse-adapted or guinea pig-adapted MARV in 100 μL of PBS. Twenty-four hours later, animals were injected with mAbs by the intraperitoneal route using 0.1 mg in 100 μL of PBS (mice) or 5 mg in 1 mL of PBS (guinea pigs) per treatment. Animals treated with the irrelevant 2D22 dengue virus-specific antibody served as controls. Animal observation procedure was performed as described in (Ilinykh et al., 2018a). The overall observation period lasted for 28 days.

For analysis of immune cells in mesenteric lymph nodes of antibody-treated animals by confocal microscopy, BALB/c mice were injected intraperitoneally with 1,000 PFU of mouse-adapted MARV in 100 μL of PBS (12 mice) or injected intraperitoneally with equal volume of PBS (6 mice). In 24 h, infected animals received 100 μg of rMR228, rMR228-LALA or MR191N in 100 μL of PBS, or equal volume of PBS (3 animals per each group); uninfected animals received 100 μg of rMR228 or MR191N in 100 μL of PBS, or equal volume of PBS (2 animals per each group). Infected mice were euthanized on days 2 or 5, uninfected – on day 5; mesenterical lymph nodes were extracted and fixed with formalin for 48 h. For flow cytometric analysis of macrophages and MARV-infected cells and titration of MARV, 15 BALB/c mice were challenged with 1,000 PFU of mouse-adapted MARV in 100 μL of PBS and 6 mice injected intraperitoneally with equal volume of PBS. In 24 h, infected animals received 100 μg of rMR228, rMR228-LALA, MR191N or 2D22 in 100 μL of PBS (3 animals in 2D22 group and 4 animals in each of the other groups); mock-infected animals received 100 μg of rMR228 or MR191N in 100 μL of PBS, or equal volume of PBS (2 animals per each group). On day 5 post-infection, these animals were euthanized, and mesenteric lymph nodes, liver, spleen and serum were collected. Serum and macerated portions of liver and spleen were titrated and lymph nodes were passed through 100 pm mesh, immunostained, and subjected to flow cytometric analysis.

METHOD DETAILS

Generation of rMR228, rMR228-KA and rMR228-LALA mAbs.—Antibody heavy- and light-chain variable region genes were sequenced from hybridoma lines that had been cloned biologically from flow cytometry. Briefly, total RNA was extracted using the RNeasy Mini kit (Qiagen) and reverse-transcriptase PCR (RT-PCR) amplification of the antibody gene cDNAs was performed using the PrimeScript One Step RT-PCR kit (Clontech) according to the manufacturer's protocol with gene-specific primers (Thornburg et al., 2016). The thermal cycling conditions were as follows: 50°C for 30 min, 94°C for 2 min, 40 cycles of (94°C for 30 s, 58°C for 30 s and 72°C for 1 min). PCR products were purified

using Agencourt AMPure XP magnetic beads (Beckman Coulter) and sequenced directly using an ABI3700 automated DNA analyzer. For recombinant mAb production, cDNA encoding the genes of heavy and light chains were cloned into DNA plasmid expression vectors encoding IgG1-, IgG1-KA- or IgG1-LALA-heavy chain (McLean et al., 2000) and transformed into *Escherichia coli* cells. MAb proteins were produced following transiently transfection of Expi293F cells following the manufacturer's protocol and were purified from filtered culture supernatants by fast protein liquid chromatography on an ÄKTA instrument using HiTrap MabSelect Sure or HiTrap Protein G columns (GE Healthcare). Purified mAbs were buffer exchanged into PBS, filtered using sterile 0.45-μm pore size filter devices (MilliporeSigma), concentrated, and stored in aliquots at −80°C until use.

Analysis of mAb IgG subclass specificity.—The isotype and subclass of secreted antibodies were determined using murine anti-human IgG1, IgG2, IgG3 or IgG4 mouse antibodies conjugated with alkaline phosphatase (Southern Biotech).

Analysis of viremia.—Serum, liver and spleen samples were kept at −80°C until analyzed for virus. For MARV titration, organ samples were weighed and homogenized in 100 μL (spleen) or 200 μL (liver) of Minimal Essential Medium supplemented with 10% FBS. The homogenates, along with serum samples, were subjected to 10-fold serial dilutions and inoculated in duplicate Vero-E6 cell monolayers. The infected monolayers were covered with 0.7% tragacanth (Spectrum Chemical) diluted in Minimal Essential Medium supplemented with 2% FBS and incubated at 37°C for 14 days. Cells were fixed in 10% phosphate-buffered formalin (ThermoFisher Scientific) for 24 h, washed thoroughly with fresh water then blocked in 5% milk in PBST buffer (0.1% Tween-20 in PBS) for 1 h. Then, cells were incubated with the human monoclonal antibodies MR235 and MR246 diluted at 0.5 μg/mL each in 5% milk/PBST for 1 h at room temperature, washed three times with PBST, and incubated with goat-anti-human IgG (γ) polyclonal antibody (KPL) conjugated with horseradish peroxidase (HRP) diluted at 1 μg/mL in 5% milk/PBST for 1 h at room temperature. Cells were washed as above, and plaques were visualized using the 4CN two-component peroxidase substrate system (KPL). The plaques were counted, and the results were expressed as PFU/g for spleen and liver samples or PFU/mL for serum samples.

Confocal microscopy analysis of lymph nodes.—Formalin-fixed mesenterical lymph nodes from euthanized mice were dehydrated in increasing ethanol concentrations, treated with xylene, paraffin-embedded and sectioned to glass slides (Mark et al., 2007). For immunofluorescence staining in paraffin sections, established protocols adapted for MARV detection were used (Santos et al., 2016). Briefly, 5 μm paraffin sections were deparaffinized in xylene and rehydrated in decreasing concentrations of ethanol and subjected to DAKO Target Retrieval Solution (Dako North America Inc.) for 15 min with microwave heating (Taylor et al., 1996). After the slides reached room temperature, samples were irradiated with UV light for 60 min for autofluorescence photobleaching (Viegas et al., 2007) and treated for an additional 10 min in 0.5 M glycine. A Mouse-On-Mouse kit (MOM-Vector labs) was used to reduce the background. Tissue samples were blocked using MOM blocking solution (Hierck et al., 1994). For MARV staining, a rabbit polyclonal antibody (IBT Bioservices) or non-immune rabbit serum (MilliporeSigma) diluted 1:100 was used,

and for immune cell staining, one of the following antibodies was used: rat anti-F4/80 for macrophages (Abcam, clone A3.1); rat anti-Ly6G for neutrophils (MilliporeSigma, clone 1A8); rat anti-CD3 for lymphocytes (Abcam, clone CD3.12); and mouse anti-NK1.1 for NK cells (MilliporeSigma, clone PK136). All primary antibodies for immune cell staining were diluted at 1:50 and incubated with samples for 60 min at room temperature. The secondary MOM biotinylated horse anti-mouse (1:250) antibody was used for NK1.1, and donkey anti-rat biotinylated IgG was used for the other immune cell markers (1:200). A donkey anti-rabbit IgG conjugated with Alexa Fluor 488 (1:200) was used for MARV staining. Secondary antibodies were incubated with samples for 40 min at room temperature. Streptavidin conjugated with Alexa Fluor 647 (1:200) was used to detect the biotin present in the anti-mouse and anti-rat antibodies. DAPI (1 μg/mL) was used as counterstaining and 0.1% Sudan Black (diluted in 70% ethanol) was used to reduce the autofluorescence properties of lipids in the tissue. Slides were analyzed by laser scanning confocal microscopy using an Olympus FV1000 confocal microscope. Lasers with 405 nm wavelengths were used for DAPI excitation, 488 nm for Alexa Fluor 488, and 635 nm for Alexa Fluor 647.

Flow cytometry analysis of macrophages and virus-infected cells in mesenteric lymph nodes.—Mesenteric lymph nodes from MARV-infected mice were passed through a 100 μm mesh with a syringe plumb, the resultant cells were washed three times with 2% FBS in PBS and stained for PerCP-Cy5.5-labeled rat anti-Ly6C mAb (clone HK1.4, BioLegend), Brilliant Violet 421-labeled rat anti-CD11b mAb (clone M1/70, BioLegend) and APC-labeled rat anti-F4/80 mAb (clone BM8, BioLegend) diluted in BD Stain Buffer (FBS) (BD Biosciences). Cells were incubated at room temperature for 20 min, washed 3 times as above and subjected to Live/Dead staining by Live/Dead Fixable Dead Cell Stain kit (ThermoFisher Scientific) following manufacturer's instructions. To also stain MARV antigens, cells were treated with BD Cytofix/Cytoperm, washed 3 times in PBS, treated with rabbit serum raised against MARV virus-like particles (IBT Bioservices) for 30 min, washed 3 times in PBS and incubated with Alexa Fluor 488-conjugated donkey anti-rabbit IgG (ThermoFisher Scientific). The cells also were fixed with 4% paraformaldehyde at room temperature for 2 h and removed from BSL-4 facility for flow cytometry analysis using a FACSCanto II instrument (BD Biosciences). Macrophages were defined as $CD11b^{high}$, $F4/80^{high}$, $Ly6C^{+}$. At least 10,000 events were acquired for each sample.

Expression of MARV and RAVV GPs.—Purified Musoke GP, Angola GP, Popp GP, RAVV GP, Musoke GPΔmuc, Angola GPΔmuc and RAVV GPΔmuc ectodomains were prepared as previously described (Fusco et al., 2015; Hashiguchi et al., 2015).

MAb binding to GP of different marburgviruses.—Wells of microtiter plates were coated with MARV or RAVV GPs and incubated at 4°C overnight. Plates were blocked with 2% non-fat dry milk and 2% normal goat serum (NGS) in Dulbecco's PBS (DPBS) containing 0.05% Tween-20 for 1 h. For dose-response analysis, serial dilutions of purified mAbs were applied to the wells in triplicate or quadruplicate in blocking buffer and incubated for 1 h at ambient temperature. The bound antibodies were detected using goat anti-human IgG conjugated with HRP (Southern Biotech) and TMB substrate

(ThermoFisher Scientific). Color development was monitored, 1N hydrochloric acid was added to stop the reaction, and the absorbance was measured at 450 nm using a spectrophotometer (Biotek). EC_{50} values for mAb binding were determined using Prism 7.2 software (GraphPad) after log transformation of antibody concentration using sigmoidal dose-response nonlinear regression analysis.

Antibody-dependent neutrophil phagocytosis.—Biotinylated recombinant MARV GP protein (strain Angola, IBT Bioservices) was coupled to yellow-green Neutravidin beads (Life Technologies). Antibodies were 5-fold serially diluted from 5 to 6.4 x 10^{-5} μg/mL in culture medium and incubated with MARV GP-coated beads for 2 h at 37°C. Freshly isolated white blood cells from peripheral blood samples of 2 different human donors were added at 5 x 10^4 cells/well and incubated for 1 h at 37°C. Cells were stained for CD66b (Clone G10F5, BioLegend), CD3 (Clone UCHT1, BD Biosciences), and CD14 (Clone MφP9, BD Biosciences), fixed with 4% paraformaldehyde, and analyzed by flow cytometry. Neutrophils were defined as SSC-A^{high} $CD66b^+$, $CD3^-$, $CD14^-$. A phagocytic score was determined using the following formula: (percentage of $FITC^+$ cells)*(geometric mean fluorescent intensity of the $FITC^+$ cells)/10,000.

Antibody-dependent THP-1 monocyte phagocytosis.—MARV GP-coated beads were generated as described for ADNP. Antibodies were 5-fold serially diluted from 5 to 3.2 x 10^{-4} μg/mL in culture medium and incubated in duplicates with MARV GP-coated beads for 2 h at 37°C. Unbound antibodies were removed by centrifugation prior to the addition of THP-1 cells at 2.5 x 10^4 cells/well. Cells were fixed with 4% paraformaldehyde and analyzed by flow cytometry. A phagocytic score was determined as described for ADNP.

Antibody-dependent primary monocyte phagocytosis.—MARV GP-coated beads were generated as described for ADNP. Antibodies were 5-fold serially diluted from 5 to 6.4 x 10^{-5} μg/mL in culture medium and incubated in triplicates with MARV GP-coated beads for 2 h at 37°C. Monocytes were enriched from human donor peripheral blood by negative selection (EasySep human monocyte enrichment kit; StemCell), and 5 x 10^4 cells/well were added to the immune complexes for 4 h at 37°C. Cells were stained for CD14 (Clone MφP9, BD Biosciences) and CD16 (Clone 3G8, BD Biosciences), fixed with 4% paraformaldehyde, and analyzed by flow cytometry. A phagocytic score was determined as described for ADNP.

Antibody-dependent neutrophil and monocyte phagocytosis with MARV-infected cells.—To validate the phagocytosis data generated with GP-covered beads using MARV-infected cells, Vero-E6 cells were seeded in 96-well plates at 20,000 cells/well and incubated for 24 h, pre-stained with CellTrace (ThermoFisher Scientific), infected with MARV strain Angola at an MOI of 6 PFU/cell and incubated for 3 more days. MAbs were diluted at 20 μg/mL in cell culture medium and incubated with MARV-infected Vero-E6 cells for 1 h at 37°C. PBMCs and granulocytes were purified from white blood cells of human donors and added atop the infected or mock-infected Vero-E6 cells at 100,000 PBMCs and 100,000 granulocytes per well. The plate was centrifuged at 350 x *g* for 5 min and incubated for 2 h at 37°C. Neutrophils were stained with PE labeled mouse anti-CD66b

(Clone G10F5, BioLegend), and monocytes were stained with BV421 labeled mouse anti-CD14 (Clone MφP9, BD Biosciences) for 15 min at room temperature. Cells were washed once with PBS and stained with Live/Dead Fixable Cell Stain kit following manufacturer's instructions. Cells were fixed with 4% paraformaldehyde as above and analyzed by flow cytometry using a FACSCanto II instrument. For each sample, at least 10,000 events were acquired. Neutrophils were defined as SSC-A^{high} CD66b^{+}, CD3^{-}, CD14^{-}, and monocytes were defined as CD3^{-} and CD14^{+}. A phagocytic score was determined using the following formula: (percentage of CellTrace^{+} cells)*(geometric mean fluorescent intensity of the CellTrace^{+} cells)/10,000.

Activation of NK cells.—MARV GP-antigen was coated onto a MaxiSorp 96-well plate (Nunc) at 300 ng/well at 4°C overnight. Wells were washed with PBS and blocked with 5% bovine serum albumin (BSA) prior to addition of antibodies diluted to 10 μg/mL, or 5-fold serially diluted from 1 to 6.4 x 10^{-5} μg/mL, for 2 h at 37°C. Unbound antibodies were removed by PBS wash, and NK cells enriched from the peripheral blood of three different human donors were added at 5 x 10^{4} cells/well in the presence of 4 μg/mL brefeldin A (MilliporeSigma), 5 μg/mL GolgiStop (Life Technologies) and anti-CD107a antibody (Clone H4A3, BD Biosciences) for 5 h. Cells were fixed and permeabilized with Fix/Perm (Life Technologies) according to the manufacturer's instructions to stain for intracellular IFNγ (Clone B27, BD Biosciences) and MIP-1β (Clone D21-1351, BD Biosciences). Cells were analyzed on an LSRII flow cytometer (BD Biosciences).

VSV/MARV-GP passaging in presence of MR228.—The escape mutant approach for identification of MARV mAb epitopes was described earlier (Flyak et al., 2015). Briefly, 200 PFU of VSV/MARV-GP were pre-incubated before each passage for 1 h at 37°C with 400 μg/mL of MR228 and passaged eight times in Vero-E6 cells in presence of 400 μg/mL of MR228, with 2 days for each passage. After the last passage, infected cell monolayer was harvested in TRIzol reagent (ThermoFisher Scientific) and subjected to total RNA isolation. MARV GP ORF was sequenced in the obtained sample.

MAb binding to mutated GP constructs.—MARV GP mutants were generated based on the Musoke strain (GenBank: DQ217792.1). The pCAGGS MCSII mammalian vector expressing wild-type MARV Musoke strain GP was provided by Dr. Christopher F. Basler (Georgia State University). Mutations were introduced by cloning of the respective gene blocks produced as a custom synthesis by IDT into the vector plasmid with T4 quick ligation kit (New England BioLabs), or using Q5 Site-Directed Mutagenesis Kit (New England BioLabs). The obtained constructs are summarized in Table S1.

The mutated GP constructs or vector containing wild-type MARV GP sequence were used to transfect triplicateHEK-293T cell monolayers maintained in high glucose Dulbecco's Minimal Essential Medium (ThermoFisher Scientific) supplemented by 10% FBS (HyClone) and 1% penicillin-streptomycin in 5% CO_2 at 37°C. Four days after transfection, cells were harvested and subjected to centrifugation at 200 x *g* for 10 min at room temperature. Supernatants were removed and cells were fixed with 4% paraformaldehyde at room temperature for 15 min. Fixed cells were washed three times with PBST and stained for 1 h at room temperature with rabbit polyclonal serum raised against MARV strain

Musoke (1:1,000; poly-Ab1) provided by Dr. Thomas G. Ksiazek (UTMB), rabbit anti-MARV GP polyclonal antibody (1:1,000; poly-Ab2; IBT Bioservices), MR228, MR235 or MR186 antibodies diluted at 10 μg/mL in FACS buffer (1% BSA and 0.5% Triton X-100 in PBS). Then, cells were washed three times with PBST and stained with secondary antibodies: goat anti-rabbit labeled with FITC (Southern Biotech) or goat anti-human labeled with Alexa Fluor 488 (Invitrogen), diluted at 5 μg/mL in FACS buffer. After 1 h of incubation at room temperature in the dark, cells were washed three times with PBST and analyzed by flow cytometry using an Accuri C6 cytometer (BD Biosciences) to determine the mean fluorescence intensity (MFI). The data were analyzed by FlowJo software, version 7.6.1 (FlowJo LLC). Antibody binding to mutated GP constructs was presented as percent of their binding to wild-type MARV GP, based on MFI values.

Peptide microarray.—168 overlapping 15 residue peptides corresponding to MARV strain 200501379 Angola GP sequence were produced by JPT Peptide Technologies GmbH (Berlin, Germany). The first peptide corresponds to residues 1 to 15 and each successive peptide begins 4 residues downstream (5 to 19, 9 to 23, etc.). The 168 peptides were spotted in triplicate to form one block of spots. MR228, MR235 and 2D22 (10 μg/mL for each mAb) were incubated for 1 h at 30°C followed by 5 washes in JPT washing buffer. One block was incubated in washing buffer as a background. All blocks were then incubated in 1 μg/mL Alexa Fluor 647-conjugated goat anti-human secondary antibody (Jackson ImmunoResearch Laboratories) followed by 5 washes in JPT washing buffer. After an additional wash in deionized water, the slide was dried by centrifugation. Median fluorescence intensity was recorded for each spot on the GenePix 4000b at 550 V and analyzed by GenePix Pro 6. The results were expressed as percent of MR228 or MR235 signal minus background to 2D22 signal minus background, for each individual peptide.

Epitope mapping using a MARV GP alanine-scan mutation library.—Comprehensive high-throughput alanine scanning (‘shotgun mutagenesis’) was carried out on an expression construct for MARV GP (strain Uganda 01Uga07 lacking MLD residues 257-425). Residues 2-256 and 426-681 were mutagenized to create a library of clones, each containing an individual GP point mutant. Non-alanine residues were changed to alanine, and alanine residues changed to serine. The resulting MARV GP alanine-scan library covered 99.8% of target residues (510 of 511). Each individual mutation was confirmed by DNA sequencing, and clones were arrayed into 384-well plates, one mutant per well.

The MARV GP mutation library was transfected into HEK-293T cells and incubated for 22 h. The immunoreactivity of each mAb was first optimized by determining reactivity with fixed or unfixed cells over a range of mAb concentrations to identify optimal signal-to-background ratios (> 5:1) and to ensure that signals were within the linear range of detection. Cells were fixed in 4% paraformaldehyde in PBS plus calcium and magnesium and then were incubated with an anti-MARV mAb diluted in 10% NGS (MilliporeSigma). The cells were incubated with anti-MARV antibody for 1 h at room temperature, followed by a 30 min incubation with Alexa Fluor 488-conjugated secondary antibody (Jackson ImmunoResearch Laboratories) in 10% NGS. Cells were washed twice with PBS without calcium or magnesium and resuspended in Cellstripper (Cellgro) plus 0.1% BSA

(MilliporeSigma). Cellular fluorescence was detected using the Intellicyt iQue high throughput flow cytometer (Sartorius). Background fluorescence was determined by fluorescence measurement of vector-transfected control cells. MAb reactivities against each mutant MARV GP clone were calculated relative to wild-type MARV GP reactivity by subtracting the signal from mock-transfected controls and normalizing to the signal from wild-type GP-transfected controls.

Mutated residues within critical clones were identified as critical to the mAb epitope if they did not support reactivity of the test mAb but did support reactivity of other control MARV mAbs. This counter-screen strategy facilitates the exclusion of GP mutants that are locally misfolded or that have an expression defect. The detailed algorithms used to interpret shotgun mutagenesis data are described elsewhere (Davidson and Doranz, 2014).

MAb binding to the cell surface displayed GP.—The assay was adapted from that of previously reported for cell surface displayed EBOV GP (Gilchuk et al., 2018). Jurkat-MARV GP or untransduced Jurkat cells were washed with the incubation buffer containing DPBS, 2% of heat-inactivated FBS and 2 mM EDTA (pH 8.0) by centrifugation at 400 x *g* for 5 min at room temperature. Binding to cell surface displayed GP was assessed with mAbs that were directly fluorescently-labeled. Briefly, mAbs were labeled with Alexa Fluor 647 NHS ester (ThermoFisher Scientific) by following the manufacturer's protocol. Labeled mAbs were purified further and buffer exchanged into the PBS using desalting Zeba columns (ThermoFisher Scientific) and stored at 4°C with 0.1% BSA (MilliporeSigma) and 0.01% sodium azide. For antibody staining, ~5 x 10^4 cells were added per each well of V-bottom 96-well plate (Corning) in 5 μL of the incubation buffer. Serial dilutions of Alexa Fluor 647-labeled antibody were added to the cells in triplicate or quadruplicate for total volume of 50 μL per well, followed by 1 h incubation at room temperature, or 4°C in some experiments. Unbound antibody was removed by washing with 200 μL of the incubation buffer as described above. Staining of cells was measured by flow cytometry using an Intellicyt iQue high throughput cytometer (Intellicyt), or an LSRII flow cytometer (BD Biosciences). Data for up to 20,000 events were acquired and analyzed with ForeCyt (Intellicyt) or FlowJo (Tree Star) software. Dead cells were excluded from the analysis on the basis of forward and side scatter gate for viable cell population. Binding to untransduced Jurkat cells served as negative controls for most experiments.

Cell surface displayed GP mAb competition-binding.—Jurkat-MARV GP cells were pre-incubated with a saturating concentration (typically 10 to 20 μg/mL) of the first unlabeled mAb at room temperature for 30 min, followed by addition of the second Alexa Fluor 647-labeled mAb (typically 5 μg/mL) and incubated for an additional 30 min. The second mAb was added after the first mAb and without washing of cells to minimize a dissociation of the first mAb from cell surface GP during a prolonged incubation. Cells were washed, fixed with 4% paraformaldehyde, and cell staining was analyzed using an Intellicyt iQue flow cytometer as detailed above. Background values were determined from binding of the second labeled mAb itself to untransduced (mock) Jurkat. Results are expressed as the percent of binding in the presence of competitor mAb relative to primary mAb-only control (maximal binding) minus background. The antibodies were considered competing if the

presence of the first antibody reduced the signal of the second antibody to less than 30% of its maximal binding or non-competing if the signal was greater than 70%.

For competition binding study with human plasma Abs, Jurkat-MARV GP cells were primed proteolytically with 0.5 mg/mL thermolysin (Pierce) in PBS for 5 min at 34°C, then washed with PBS containing 2% of FBS and 2 mM EDTA (pH 8.0). For staining, cells were incubated for 30 min at 4°C with serial 3-fold dilutions of a MARV survivor plasma (Flyak et al., 2015) starting from 1:50 dilution in triplicate, followed by incubation for 30 min with 5 μg/mL of respective Alexa Fluor 647-labeled MARV GP-specific mAb. Cells were washed, fixed with 4% paraformaldehyde in PBS, and analyzed using Intellicyt iQue flow cytometer as detailed above. Plasma from a donor without an exposure history to filovirus infection was used as a negative control. Background values were determined from binding of second labeled antibody to untransfected Jurkat cells. Results were expressed as the percentages of MARV GP-reactive antibody binding in the presence of plasma relative to a MARV-specific mAb-only control (maximal binding), minus background.

Cooperative binding to cell surface displayed GP.—The cell surface display assay was based on principles from previously described enhanced binding ELISA assay (Howell et al., 2017). Briefly, Jurkat-MARV GP cells were incubated in replicates with Alexa Fluor 647-labeled RBS-specific mAbs MR78 or MR191 alone, or with Alexa Fluor 647-labeled MR78 or MR191 titrated into a fixed saturating concentration of wing-specific mAb MR235 or control mAb 2D22. Cells were washed, and antibody binding was analyzed by flow cytometry using Intellicyt iQue.

***In vitro* neutralization assay.—**Aliquots of EBOV/MARV-GP were pre-incubated for 1 h in 5% CO_2 at 37°C with serial 4-fold dilutions of mAbs, with or without guinea pig complement (MP Biomedicals), and inoculated into Vero-E6 triplicate monolayers in black polystyrene 96-well plates with clear bottoms (Corning). The final amount of virus was 1,000 PFU, the starting concentration of mAbs 200 μg/mL for the single mAbs and 100 μg/mL for each of the two mAbs in combination (200 μg/mL of the total mAb) and complement concentration 10% (v/v). Cells were maintained in Minimal Essential Medium (ThermoFisher Scientific) supplemented by 10% FBS (HyClone) and 1% penicillin-streptomycin in 5% CO_2 at 37°C. After 4 days of incubation, fluorescence intensity of infected cells was measured at a 488 nm wavelength using a 2104 EnVision multilabel reader (Perkin-Elmer). The signal readout was normalized to virus control aliquots with no mAb added and was presented as the percentage of neutralization.

Western blot analysis of antigen recognition by MR228 and MR235 mAbs.—One microgram aliquots of purified MARV or RAVV GP protein constructs were equilibrated with NuPAGE LDS Sample Buffer (ThermoFisher Scientific) for non-reducing conditions, or equilibrated with NuPAGE LDS Sample Buffer, reduced by addition of DTT up to a final concentration of 50 mM, and heated at 95°C for 5 min for reducing conditions. The samples were resolved on SDS-PAGE gels and transferred on to polyvinylidene difluoride membranes (MilliporeSigma). The membranes were blocked with 5% milk and 0.05% Tween-20 in PBS for 1 h at ambient temperature and probed overnight at 4°C with MR228 or MR235 antibodies diluted to 1 μg/mL in 3% milk and 0.05% Tween-20 in PBS.

Next, the membranes were washed 3 times in PBS with 0.05% Tween-20, and incubated with goat anti-human IgG Fc-HRP secondary antibody (Invitrogen) diluted at 1:5,000 in 3% milk and 0.05% Tween-20 in PBS for 1 h at ambient temperature. The protein bands were visualized using ECL substrate (ThermoFisher Scientific).

QUANTIFICATION AND STATISTICAL ANALYSIS

Statistical analyses and generation of graphs were performed using GraphPad Prism version 6.05 (GraphPad Software). One-Way ANOVA and two-sided unpaired Student's t-test were used for statistical analysis of *in vitro* data. Animal survival data were analyzed by log-rank (Mantel-Cox) test. The details of quantitative data analysis for mAb binding to GP of different marburgviruses, effector functions in response to stimulation with recombinant MARV GP or MARV infection, mAb binding to mutated GP constructs, peptide microarray, epitope mapping using a MARV GP alanine-scan mutation library, mAb binding and competition-binding to the cell surface displayed GP are included in the respective subsections of STAR Methods. The synergistic effects based on the mean fluorescence reduction in neutralization test were evaluated by the formula proposed by Spector et al. (Spector et al., 1982). Briefly, the combination index (CI) was calculated by formula ln(mAb1) + ln(mAb2) − ln(mAb1 + mAb2) − ln(control), where "mAb1" represents MFI of cells infected in presence of MR235 or MR228 alone, "mAb2" − MFI of cells infected in presence of neutralizing antibody only (without MR235 or MR228), "mAbl + mAb2" − MFI of cells infected under combination of the corresponding mAbs, and "control" − MFI of infected cells with no mAb added. When CI > 0 + 2 SE, it was considered indicative of the mAb synergism. The statistical details of experiments, including the exact method used, number of biological and/or technical replicates, number of animals and definition of p values are included in the figure legends. No methods were used to determine whether the data met assumptions of the statistical approach.

DATA AND CODE AVAILABILITY

Source data for Figures 3B,C and S4C are available at Mendeley Data at https://data.mendeley.com/datasets/yrhzkttr73/1 and https://data.mendeley.com/datasets/b8ckvvdmr6/1, respectively. All other datasets generated during and/or analyzed during the current study are available from the Lead Contact on reasonable request.

Supplementary Material

Refer to Web version on PubMed Central for supplementary material.

ACKNOWLEDGEMENTS

We thank the UTMB Animal Resource Center veterinary staff for the excellent technical support of *in vivo* experiments in the ABSL-4. We thank Dr. James Zhu (USDA) for assisting with the peptide microarray. This project was funded by the U.S. NIH grants U19 AI109711 and U19 AI142785 (to JEC and AB) and Defense Threat Reduction Agency grant HDTRA1-13-1-0034 (to JEC and AB). NIH contract HHSN 75N93019C00073 supported epitope mapping at Integral Molecular.

REFERENCES

Alter G, Malenfant JM, and Altfeld M (2004). CD107a as a functional marker for the identification of natural killer cell activity. J Immunol Methods 294, 15–22. [PubMed: 15604012]

Amarasinghe GK, Bao Y, Basler CF, Bavari S, Beer M, Bejerman N, Blasdell KR, Bochnowski A, Briese T, Bukreyev A, et al. (2017). Taxonomy of the order Mononegavirales: update 2017. Arch Virol 162, 2493–2504. [PubMed: 28389807]

Baize S, Leroy EM, Mavoungou E, and Fisher-Hoch SP (2000). Apoptosis in fatal Ebola infection. Does the virus toll the bell for immune system? Apoptosis 5, 5–7. [PubMed: 11227491]

Bornholdt ZA, Ndungo E, Fusco ML, Bale S, Flyak AI, Crowe JE Jr., Chandran K, and Saphire EO (2016). Host-Primed Ebola Virus GP Exposes a Hydrophobic NPC1 Receptor-Binding Pocket, Revealing a Target for Broadly Neutralizing Antibodies. MBio 7, e02154–02115. [PubMed: 26908579]

Bramble MS, Hoff N, Gilchuk P, Mukadi P, Lu K, Doshi RH, Steffen I, Nicholson BP, Lipson A, Vashist N, et al. (2018). Pan-Filovirus Serum Neutralizing Antibodies in a Subset of Congolese Ebolavirus Infection Survivors. J Infect Dis.

Bruhns P, Iannascoli B, England P, Mancardi DA, Fernandez N, Jorieux S, and Daeron M (2009). Specificity and affinity of human Fcgamma receptors and their polymorphic variants for human IgG subclasses. Blood 113, 3716–3725. [PubMed: 19018092]

Bukreyev A, Volchkov VE, Blinov VM, and Netesov SV (1993). The GP-protein of Marburg virus contains the region similar to the ‘immunosuppressive domain’ of oncogenic retrovirus P15E proteins. FEBS Lett 323, 183–187. [PubMed: 8495737]

Burk R, Bollinger L, Johnson JC, Wada J, Radoshitzky SR, Palacios G, Bavari S, Jahrling PB, and Kuhn JH (2016). Neglected filoviruses. FEMS Microbiol Rev 40, 494–519. [PubMed: 27268907]

Carette JE, Raaben M, Wong AC, Herbert AS, Obernosterer G, Mulherkar N, Kuehne AI, Kranzusch PJ, Griffin AM, Ruthel G, et al. (2011). Ebola virus entry requires the cholesterol transporter Niemann-Pick C1. Nature 477, 340–343. [PubMed: 21866103]

CDC (2014). Known Cases and Outbreaks of Marburg Hemorrhagic Fever, in Chronological Order. http://www.cdc.gov/vhf/marburg/resources/outbreak-table.html.

Chandran K, Sullivan NJ, Felbor U, Whelan SP, and Cunningham JM (2005). Endosomal proteolysis of the Ebola virus glycoprotein is necessary for infection. Science 308, 1643–1645. [PubMed: 15831716]

Cote M, Misasi J, Ren T, Bruchez A, Lee K, Filone CM, Hensley L, Li Q, Ory D, Chandran K, et al. (2011). Small molecule inhibitors reveal Niemann-Pick C1 is essential for Ebola virus infection. Nature 477, 344–348. [PubMed: 21866101]

Davidson E, and Doranz BJ (2014). A high-throughput shotgun mutagenesis approach to mapping B-cell antibody epitopes. Immunology 143, 13–20. [PubMed: 24854488]

Davis CW, Jackson KJL, McElroy AK, Halfmann P, Huang J, Chennareddy C, Piper AE, Leung Y, Albarino CG, Crozier I, et al. (2019). Longitudinal Analysis of the Human B Cell Response to Ebola Virus Infection. Cell.

Dube D, Brecher MB, Delos SE, Rose SC, Park EW, Schornberg KL, Kuhn JH, and White JM (2009). The primed ebolavirus glycoprotein (19-kilodalton GP1,2): sequence and residues critical for host cell binding. Journal of virology 83, 2883–2891. [PubMed: 19144707]

Feldmann H, Will C, Schikore M, Slenczka W, and Klenk HD (1991). Glycosylation and oligomerization of the spike protein of Marburg virus. Virology 182, 353–356. [PubMed: 2024471]

Fibriansah G, Ibarra KD, Ng TS, Smith SA, Tan JL, Lim XN, Ooi JS, Kostyuchenko VA, Wang J, de Silva AM, et al. (2015). Cryo-EM structure of an antibody that neutralizes dengue virus type 2 by locking E protein dimers. Science 349, 88–91. [PubMed: 26138979]

Flyak AI, Ilinykh PA, Murin CD, Garron T, Shen X, Fusco ML, Hashiguchi T, Bornholdt ZA, Slaughter JC, Sapparapu G, et al. (2015). Mechanism of human antibody-mediated neutralization of Marburg virus. Cell 160, 893–903. [PubMed: 25723164]

Flyak AI, Kuzmina N, Murin CD, Bryan C, Davidson E, Gilchuk P, Gulka CP, Ilinykh PA, Shen X, Huang K, et al. (2018). Broadly neutralizing antibodies from human survivors target a conserved

site in the Ebola virus glycoprotein HR2-MPER region. Nat Microbiol 3, 670–677. [PubMed: 29736037]

Flyak AI, Shen X, Murin CD, Turner HL, David JA, Fusco ML, Lampley R, Kose N, Ilinykh PA, Kuzmina N, et al. (2016). Cross-Reactive and Potent Neutralizing Antibody Responses in Human Survivors of Natural Ebolavirus Infection. Cell 164, 392–405. [PubMed: 26806128]

Fusco ML, Hashiguchi T, Cassan R, Biggins JE, Murin CD, Warfield KL, Li S, Holtsberg FW, Shulenin S, Vu H, et al. (2015). Protective mAbs and Cross-Reactive mAbs Raised by Immunization with Engineered Marburg Virus GPs. PLoS Pathog 11, e1005016. [PubMed: 26115029]

Geisbert TW, Hensley LE, Larsen T, Young HA, Reed DS, Geisbert JB, Scott DP, Kagan E, Jahrling PB, and Davis KJ (2003). Pathogenesis of Ebola hemorrhagic fever in cynomolgus macaques: evidence that dendritic cells are early and sustained targets of infection. Am J Pathol 163, 2347–2370. [PubMed: 14633608]

Gilchuk P, Kuzmina N, Ilinykh PA, Huang K, Gunn BM, Bryan A, Davidson E, Doranz BJ, Turner HL, Fusco ML, et al. (2018). Multifunctional Pan-ebolavirus Antibody Recognizes a Site of Broad Vulnerability on the Ebolavirus Glycoprotein. Immunity 49, 363–374 e310. [PubMed: 30029854]

Gnirss K, Kuhl A, Karsten C, Glowacka I, Bertram S, Kaup F, Hofmann H, and Pohlmann S (2012). Cathepsins B and L activate Ebola but not Marburg virus glycoproteins for efficient entry into cell lines and macrophages independent of TMPRSS2 expression. Virology 424, 3–10. [PubMed: 22222211]

Goldstein T, Anthony SJ, Gbakima A, Bird BH, Bangura J, Tremeau-Bravard A, Belaganahalli MN, Wells HL, Dhanota JK, Liang E, et al. (2018). The discovery of Bombali virus adds further support for bats as hosts of ebolaviruses. Nat Microbiol.

Gunn BM, Yu WH, Karim MM, Brannan JM, Herbert AS, Wec AZ, Halfmann PJ, Fusco ML, Schendel SL, Gangavarapu K, et al. (2018). A Role for Fc Function in Therapeutic Monoclonal Antibody-Mediated Protection against Ebola Virus. Cell Host Microbe 24, 221–233 e225. [PubMed: 30092199]

Hashiguchi T, Fusco ML, Bornholdt ZA, Lee JE, Flyak AI, Matsuoka R, Kohda D, Yanagi Y, Hammel M, Crowe JE Jr., et al. (2015). Structural basis for Marburg virus neutralization by a cross-reactive human antibody. Cell 160, 904–912. [PubMed: 25723165]

Henry Dunand CJ, Leon PE, Huang M, Choi A, Chromikova V, Ho IY, Tan GS, Cruz J, Hirsh A, Zheng NY, et al. (2016). Both Neutralizing and Non-Neutralizing Human H7N9 Influenza Vaccine-Induced Monoclonal Antibodies Confer Protection. Cell Host Microbe 19, 800–813. [PubMed: 27281570]

Hessell AJ, Hangartner L, Hunter M, Havenith CE, Beurskens FJ, Bakker JM, Lanigan CM, Landucci G, Forthal DN, Parren PW, et al. (2007). Fc receptor but not complement binding is important in antibody protection against HIV. Nature 449, 101–104. [PubMed: 17805298]

Hezareh M, Hessell AJ, Jensen RC, van de Winkel JG, and Parren PW (2001). Effector function activities of a panel of mutants of a broadly neutralizing antibody against human immunodeficiency virus type 1. J Virol 75, 12161–12168. [PubMed: 11711607]

Hierck BP, Iperen LV, Gittenberger-De Groot AC, and Poelmann RE (1994). Modified indirect immunodetection allows study of murine tissue with mouse monoclonal antibodies. J Histochem Cytochem 42, 1499–1502. [PubMed: 7930532]

Holmes EC, Dudas G, Rambaut A, and Andersen KG (2016). The evolution of Ebola virus: Insights from the 2013-2016 epidemic. Nature 538, 193–200. [PubMed: 27734858]

Howell KA, Brannan JM, Bryan C, McNeal A, Davidson E, Turner HL, Vu H, Shulenin S, He S, Kuehne A, et al. (2017). Cooperativity Enables Non-neutralizing Antibodies to Neutralize Ebolavirus. Cell Rep 19, 413–424. [PubMed: 28402862]

Ilinykh PA, Graber J, Kuzmina NA, Huang K, Ksiazek TG, Crowe JE Jr., and Bukreyev A (2018a). Ebolavirus Chimerization for the Development of a Mouse Model for Screening of Bundibugyo-Specific Antibodies. J Infect Dis 218, S418–S422. [PubMed: 30060231]

Ilinykh PA, Santos RI, Gunn BM, Kuzmina NA, Shen X, Huang K, Gilchuk P, Flyak AI, Younan P, Alter G, et al. (2018b). Asymmetric antiviral effects of ebolavirus antibodies targeting glycoprotein stem and glycan cap. PLoS Pathog 14, e1007204. [PubMed: 30138408]

Ilinykh PA, Shen X, Flyak AI, Kuzmina N, Ksiazek TG, Crowe JE Jr., and Bukreyev A (2016). Chimeric Filoviruses for Identification and Characterization of Monoclonal Antibodies. J Virol 90, 3890–3901. [PubMed: 26819310]

Jacobsen FW, Stevenson R, Li C, Salimi-Moosavi H, Liu L, Wen J, Luo Q, Daris K, Buck L, Miller S, et al. (2017). Engineering an IgG Scaffold Lacking Effector Function with Optimized Developability. J Biol Chem 292, 1865–1875. [PubMed: 27994062]

Kajihara M, Marzi A, Nakayama E, Noda T, Kuroda M, Manzoor R, Matsuno K, Feldmann H, Yoshida R, Kawaoka Y, et al. (2012). Inhibition of Marburg virus budding by nonneutralizing antibodies to the envelope glycoprotein. J Virol 86, 13467–13474. [PubMed: 23035224]

Kajihara M, Nakayama E, Marzi A, Igarashi M, Feldmann H, and Takada A (2013). Novel mutations in Marburg virus glycoprotein associated with viral evasion from antibody mediated immune pressure. J Gen Virol 94, 876–883. [PubMed: 23288419]

King LB, Fusco ML, Flyak AI, Ilinykh PA, Huang K, Gunn B, Kirchdoerfer RN, Hastie KM, Sangha A, Meiler J, et al. (2018). The Marburgvirus-neutralizing human monoclonal antibody MR191 against targets a conserved site to block receptor binding. Cell Host & Microbe 23, 101–109 e104. [PubMed: 29324225]

Kuzmina NA, Younan P, Gilchuk P, Santos RI, Flyak AI, Ilinykh PA, Huang K, Lubaki NM, Ramanathan P, Crowe JE Jr., et al. (2018). Antibody-Dependent Enhancement of Ebola Virus Infection by Human Antibodies Isolated from Survivors. Cell Rep 24, 1802–1815 e1805. [PubMed: 30110637]

Lee JE, Fusco ML, Hessell AJ, Oswald WB, Burton DR, and Saphire EO (2008). Structure of the Ebola virus glycoprotein bound to an antibody from a human survivor. Nature 454, 177–182. [PubMed: 18615077]

Leon PE, He W, Mullarkey CE, Bailey MJ, Miller MS, Krammer F, Palese P, and Tan GS (2016). Optimal activation of Fc-mediated effector functions by influenza virus hemagglutinin antibodies requires two points of contact. Proc Natl Acad Sci U S A 113, E5944–E5951. [PubMed: 27647907]

Malherbe H, and Strickland-Cholmley M (1968). Human disease from monkeys (Marburg virus). Lancet 1, 1434.

Mark M, Teletin M, Antal C, Wendling O, Auwerx J, Heikkinen S, Khetchoumian K, Argmann CA, and Dgheem M (2007). Histopathology in mouse metabolic investigations. Curr Protoc Mol Biol Chapter 29, Unit 29B 24.

McLean GR, Nakouzi A, Casadevall A, and Green NS (2000). Human and murine immunoglobulin expression vector cassettes. Mol Immunol 37, 837–845. [PubMed: 11257305]

Mire CE, Geisbert JB, Borisevich V, Fenton KA, Agans KN, Flyak AI, Deer DJ, Steinkellner H, Bohorov O, Bohorova N, et al. (2017). Therapeutic treatment of Marburg and Ravn virus infection in nonhuman primates with a human monoclonal antibody. Sci Transl Med 9, pii: eaai8711.

Misasi J, Chandran K, Yang JY, Considine B, Filone CM, Cote M, Sullivan N, Fabozzi G, Hensley L, and Cunningham J (2012). Filoviruses require endosomal cysteine proteases for entry but exhibit distinct protease preferences. J Virol 86, 3284–3292. [PubMed: 22238307]

Mittler E, Kolesnikova L, Herwig A, Dolnik O, and Becker S (2013). Assembly of the Marburg virus envelope. Cell Microbiol 15, 270–284. [PubMed: 23186212]

Mullarkey CE, Bailey MJ, Golubeva DA, Tan GS, Nachbagauer R, He W, Novakowski KE, Bowdish DM, Miller MS, and Palese P (2016). Broadly Neutralizing Hemagglutinin Stalk-Specific Antibodies Induce Potent Phagocytosis of Immune Complexes by Neutrophils in an Fc-Dependent Manner. MBio 7, e01624–01616. [PubMed: 27703076]

Sanchez A, Trappier SG, Mahy BW, Peters CJ, and Nichol ST (1996). The virion glycoproteins of Ebola viruses are encoded in two reading frames and are expressed through transcriptional editing. Proc Natl Acad Sci U S A 93, 3602–3607. [PubMed: 8622982]

Santos RI, Hermance ME, Gelman BB, and Thangamani S (2016). Spinal Cord Ventral Horns and Lymphoid Organ Involvement in Powassan Virus Infection in a Mouse Model. Viruses 8.

Schornberg K, Matsuyama S, Kabsch K, Delos S, Bouton A, and White J (2006). Role of endosomal cathepsins in entry mediated by the Ebola virus glycoprotein. J Virol 80, 4174–4178. [PubMed: 16571833]

Shedlock DJ, Aviles J, Talbott KT, Wong G, Wu SJ, Villarreal DO, Myles DJ, Croyle MA, Yan J, Kobinger GP, et al. (2013). Induction of broad cytotoxic T cells by protective DNA vaccination against Marburg and Ebola. Mol Ther 21, 1432–1444. [PubMed: 23670573]

Spector SA, Tyndall M, and Kelley E (1982). Effects of acyclovir combined with other antiviral agents on human cytomegalovirus. Am J Med 73, 36–39. [PubMed: 6179416]

Taylor CR, Shi SR, Chen C, Young L, Yang C, and Cote RJ (1996). Comparative study of antigen retrieval heating methods: microwave, microwave and pressure cooker, autoclave, and steamer. Biotech Histochem 71, 263–270. [PubMed: 8896801]

Thornburg NJ, Zhang H, Bangaru S, Sapparapu G, Kose N, Lampley RM, Bombardi RG, Yu Y, Graham S, Branchizio A, et al. (2016). H7N9 influenza virus neutralizing antibodies that possess few somatic mutations. J Clin Invest 126, 1482–1494. [PubMed: 26950424]

Towner JS, Khristova ML, Sealy TK, Vincent MJ, Erickson BR, Bawiec DA, Hartman AL, Comer JA, Zaki SR, Stroher U, et al. (2006). Marburgvirus genomics and association with a large hemorrhagic fever outbreak in Angola. J Virol 80, 6497–6516. [PubMed: 16775337]

Viegas MS, Martins TC, Seco F, and do Carmo A (2007). An improved and cost-effective methodology for the reduction of autofluorescence in direct immunofluorescence studies on formalin-fixed paraffin-embedded tissues. Eur J Histochem 51, 59–66.

Volchkov VE, Becker S, Volchkova VA, Ternovoj VA, Kotov AN, Netesov SV, and Klenk HD (1995). GP mRNA of Ebola virus is edited by the Ebola virus polymerase and by T7 and vaccinia virus polymerases. Virology 214, 421–430. [PubMed: 8553543]

Volchkov VE, Volchkova VA, Stroher U, Becker S, Dolnik O, Cieplik M, Garten W, Klenk HD, and Feldmann H (2000). Proteolytic processing of Marburg virus glycoprotein. Virology 268, 1–6. [PubMed: 10683320]

Warfield KL, Alves DA, Bradfute SB, Reed DK, VanTongeren S, Kalina WV, Olinger GG, and Bavari S (2007). Development of a model for marburgvirus based on severe-combined immunodeficiency mice. Virology journal 4, 108. [PubMed: 17961252]

Will C, Muhlberger E, Linder D, Slenczka W, Klenk HD, and Feldmann H (1993). Marburg virus gene 4 encodes the virion membrane protein, a type I transmembrane glycoprotein. Journal of virology 67, 1203–1210. [PubMed: 8437211]

Wines BD, Powell MS, Parren PW, Barnes N, and Hogarth PM (2000). The IgG Fc contains distinct Fc receptor (FcR) binding sites: the leukocyte receptors Fc gamma RI and Fc gamma Rlla bind to a region in the Fc distinct from that recognized by neonatal FcR and protein A. J Immunol 164, 5313–5318. [PubMed: 10799893]

Wong G, Qiu X, Olinger GG, and Kobinger GP (2014). Post-exposure therapy of filovirus infections. Trends Microbiol 22, 456–463. [PubMed: 24794572]

Zeitlin L, Pettitt J, Scully C, Bohorova N, Kim D, Pauly M, Hiatt A, Ngo L, Steinkellner H, Whaley KJ, et al. (2011). Enhanced potency of a fucose-free monoclonal antibody being developed as an Ebola virus immunoprotectant. Proc Natl Acad Sci U S A 108, 20690–20694. [PubMed: 22143789]

Highlights

- A non-neutralizing mAb MR228 protects animals from lethal infection with Marburg virus
- MR228 binds to an epitope in the wing region of Marburg virus glycoprotein
- MR228 induces strong Fc domain-mediated effector functions
- Non-neutralizing mAb MR235 increases neutralizing mAb binding to enhance neutralization

Group	mAb	IgG Isotype	Level of protection in lethal mouse model (% animals survived)	IC_{50} value for neutralization of indicated virus (μg/mL)		EC_{50} value for binding in ELISA to GP of indicated strain (ng/mL)				Fc-mediated functions		
										Phagocytosis (mean phagocytic score)		Activation (the sum of average percent of cells positive for CD107a, IFNγ and MIP-1β)
				VSV/ MARV-GP	MARV	Musoke	Angola	Popp	RAVV	Neutrophils*	THP-1 monocytes**	NK cells
1	MR73	IgG1	0	>	>	21,262	4,810	15,545	8,080	23	20	6
	MR114	IgG1	20	>	>	2,319	991	2,189	1,109	16	24	8
	MR237	IgG1	0	>	>	2,626	879	1,127	1,060	15	24	12
2	MR228	IgG1	100	>	>	14	8.6	12	20,261	38	47	16
	MR235	IgG1	0	>	>	1.7	1.6	2.2	2.0	37	55	25
3A	MR162	IgG1	0	>	>	72	21	19	18	19	29	10
	MR221	IgG3	0	>	>	4.5	3.8	4.0	4.3	32	47	6
	MR246	IgG2	0	>	>	4.3	3.6	4.3	4.6	22	24	6
3B	MR65	IgG1	100	224	>	2,575	2,658	2,111	1,791	24	21	7
	MR72	IgG1	100	13	601	363	673	454	377	22	23	7
	MR78	IgG1	100	5	93	292	497	387	304	25	25	7
	MR79	IgG1	0	>	>	1,419	2,447	2,414	1,651	20	24	6
	MR82	IgG1	100	7	288	209	286	198	190	23	27	6
	MR103	IgG1	80	28	291	2,903	4,611	3,067	2,375	18	27	8
	MR111	IgG1	60	8	414	391	536	321	307	18	23	8
	MR144	IgG1	20	37	>	1,028	1,499	844	952	18	25	7
	MR186	IgG1	100	2	>	254	155	52	91	19	23	7
	MR191	IgG1	80	6	>	395	343	125	182	17	28	9
	MR198	IgG1	80	12	206	221	162	68	109	19	28	9
	MR201	IgG1	80	8	572	299	223	85	146	18	26	15
	MR208	IgG1	60	55	>	863	656	219	423	18	24	13
	MR209	IgG1	100	12	402	378	296	108	200	15	27	7
	MR213	IgG1	80	10	305	425	305	109	174	16	25	7
	MR229	IgG1	100	7	215	632	375	138	217	15	27	9
	MR232	IgG1	100	4	114	393	227	95	117	16	30	16
	MR238	IgG1	100	10	>	1,181	1,044	368	591	15	26	7
	MR241	IgG1	100	12	>	342	245	90	130	16	26	6

Fig. 1. Summary of mAb properties.

Four different shades of color indicate level of activity, with the most intense color corresponding to the highest level of activity for each parameter tested. White indicates activity was not detected. IC_{50} values greater than 1,000 μg/mL are indicated by >. * shown for representative mAb concentration of 1 μg/mL; ** shown for representative mAb concentration of 0.04 μg/mL.

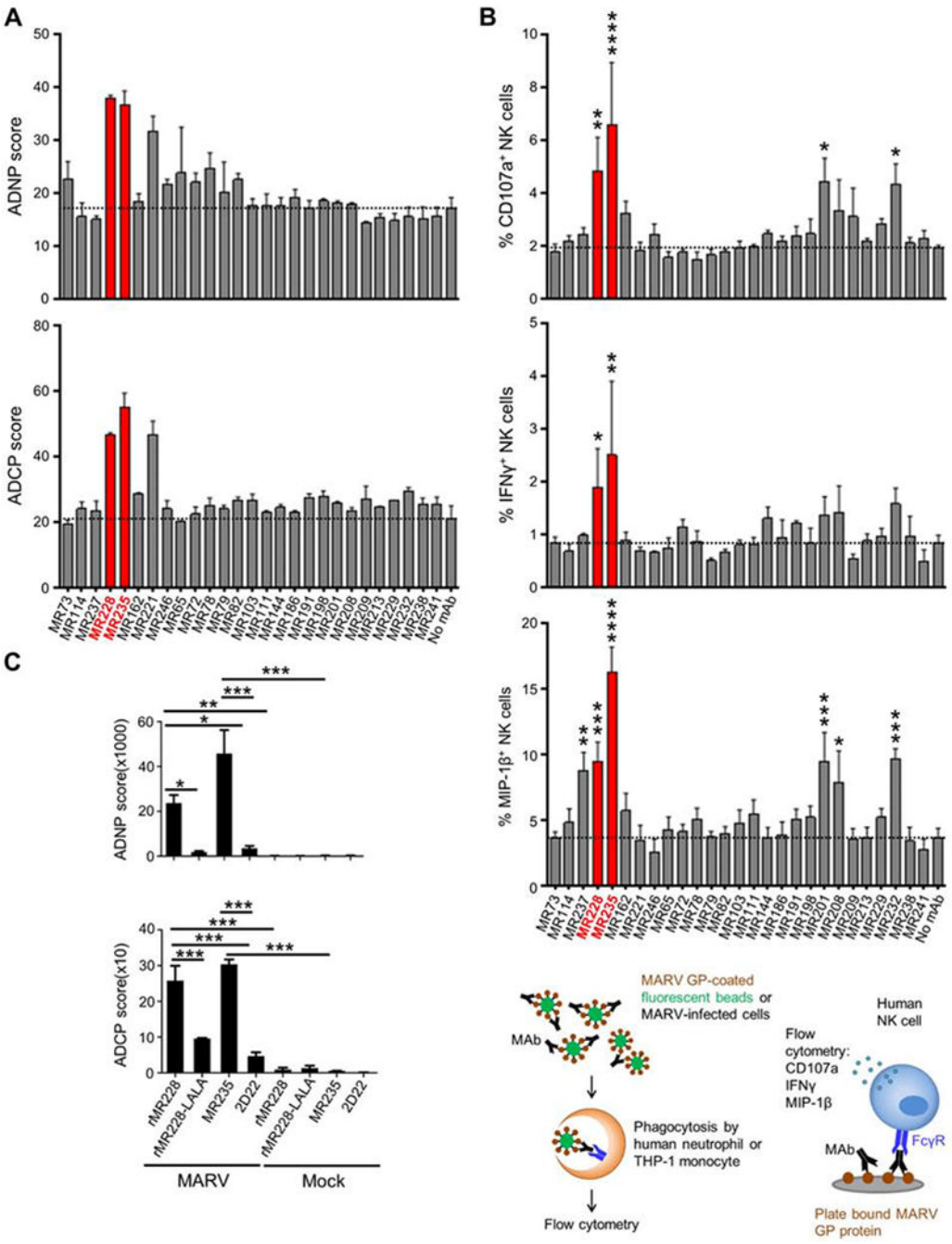

Fig. 2. Wing-specific antibodies induce strong Fc-mediated effects.

Assessing phagocytic activity of neutrophils (shown for mAb concentration of 1 μg/mL) or THP-1 monocytes (shown for mAb concentration of 0.04 μg/mL) **(A)**, or activation markers CD107a, IFNγ, MIP-1β of NK cells (shown for mAb concentration of 10 μg/mL) **(B)**, in response to incubation with mAb/MARV GP complexes, and validation of the data with MARV-infected Vero-E6 cells **(C)**. Data are shown as a mean of duplicates ± SD using neutrophils from two donors or technical replicates (THP-1 cells) (A), as a mean of triplicate measurements ± SEM using NK cells from three donors (B), as a mean of technical

quadruplicates ± SEM using neutrophils and monocytes from two donors. Data for one of two donors analyzed shown (C). Bars for the two wing-specific non-neutralizing mAbs MR228 and MR235 are highlighted in red. Dashed lines indicate no mAb levels. P values were calculated by One-Way ANOVA compared to no mAb control (Fisher LSD test, panel B) or irrelevant mAb (Tukey's correction for multiple comparison testing, panels C, D): * $p < 0.05$, ** $p < 0.01$, *** $p < 0.001$, **** $p < 0.0001$. Cartoons represent the schemes of bead-based phagocytosis and NK cell activation assays.

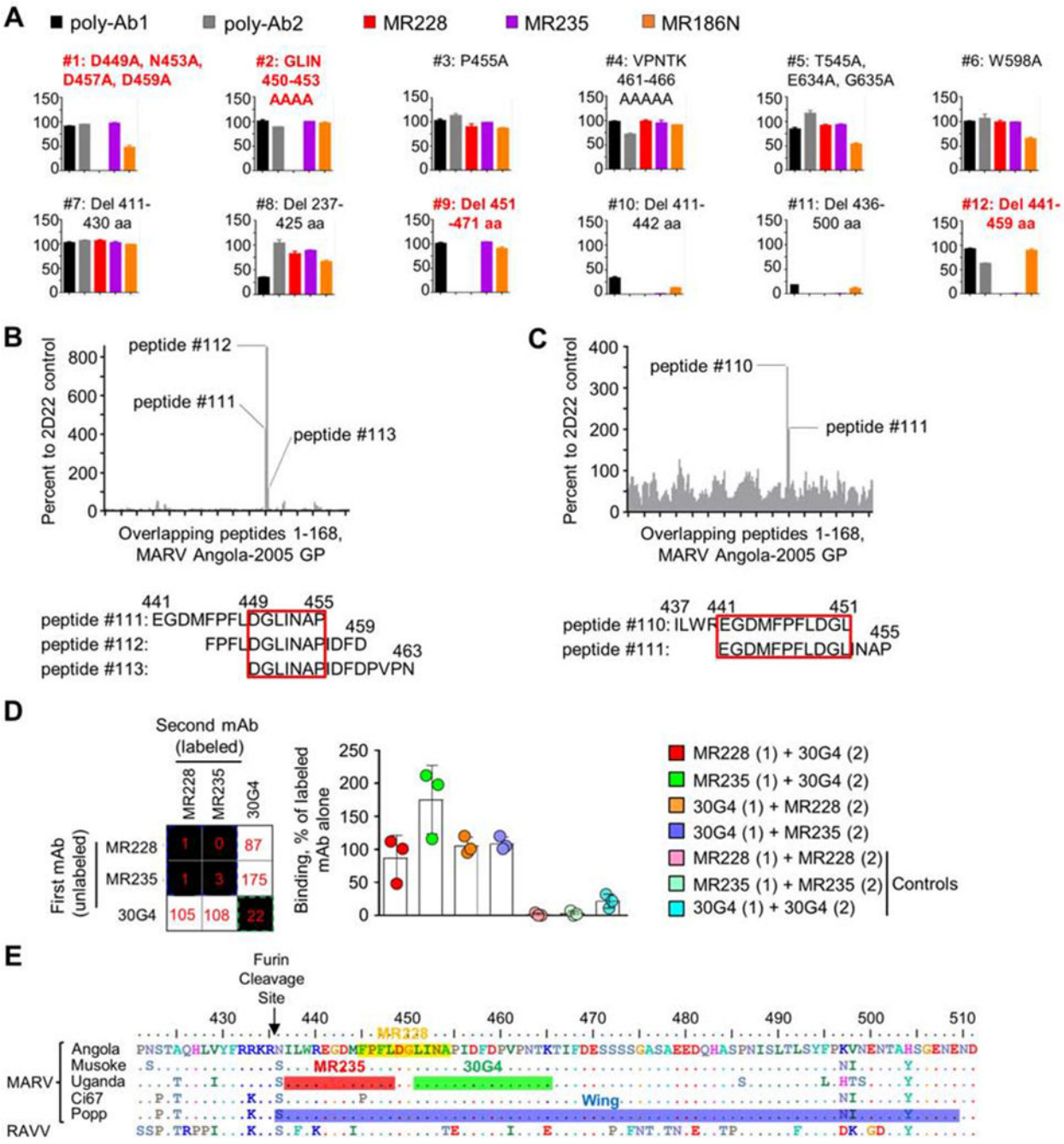

Fig. 3. MR228 and MR235 epitopes are located in GP2 wing.

(A) Epitope mapping of mAbs by flow cytometric analysis of their binding to GP constructs #1-12 with single or multiple mutations and/or deletions. The constructs which demonstrated a reduced binding of a specific mAb, but not of another mAb or reference polyclonal antibodies, to a mutated GP, are highlighted in red. Percentages of mAb binding to mutated GP normalized to non-mutated GP, which are set to 100%, are shown (mean values ± SD). The assays were performed in triplicate. As mutations in the 597-608 aa region (see Table S1) did not result in a substantial binding change, flow cytometry data for

only one representative W598A mutant are shown. **(B, C)** Identification of epitopes for MR228 (B) or MR235 (C) by peptide microarray. Each column represents MFI of a 15 residue peptide matching to the sequence of MARV GP. Each peptide was printed on the slide in triplicate for each of the analyzed samples; mean values are shown. After subtraction of the background (no primary antibody added), the signals were normalized to corresponding MFI values of the 2D22 control. The overlapping parts of the peptides that raised the highest signals are highlighted with red frames. **(D)** Neither MR228 nor MR235 competed with 30G4 mAb for GP binding. Jurkat-MARV GP or untransduced Jurkat cells were incubated with the unlabeled first mAb, then incubated with the second Alexa Fluor 647 labeled mAb and analyzed by flow cytometry. Mean values ± SD of triplicate samples are shown. **(E)** The proposed epitope sequences based on the peptide microarray and binding to mutagenized GPs; the previously published 30G4 mAb is included for comparison (from Fusco et al., 2015). MR228 (yellow, 445-454 aa) and MR235 (red, 437-448 aa) epitopes are located in GP2 wing region (blue), but differ from that of 30G4 (green, 451-465 aa).

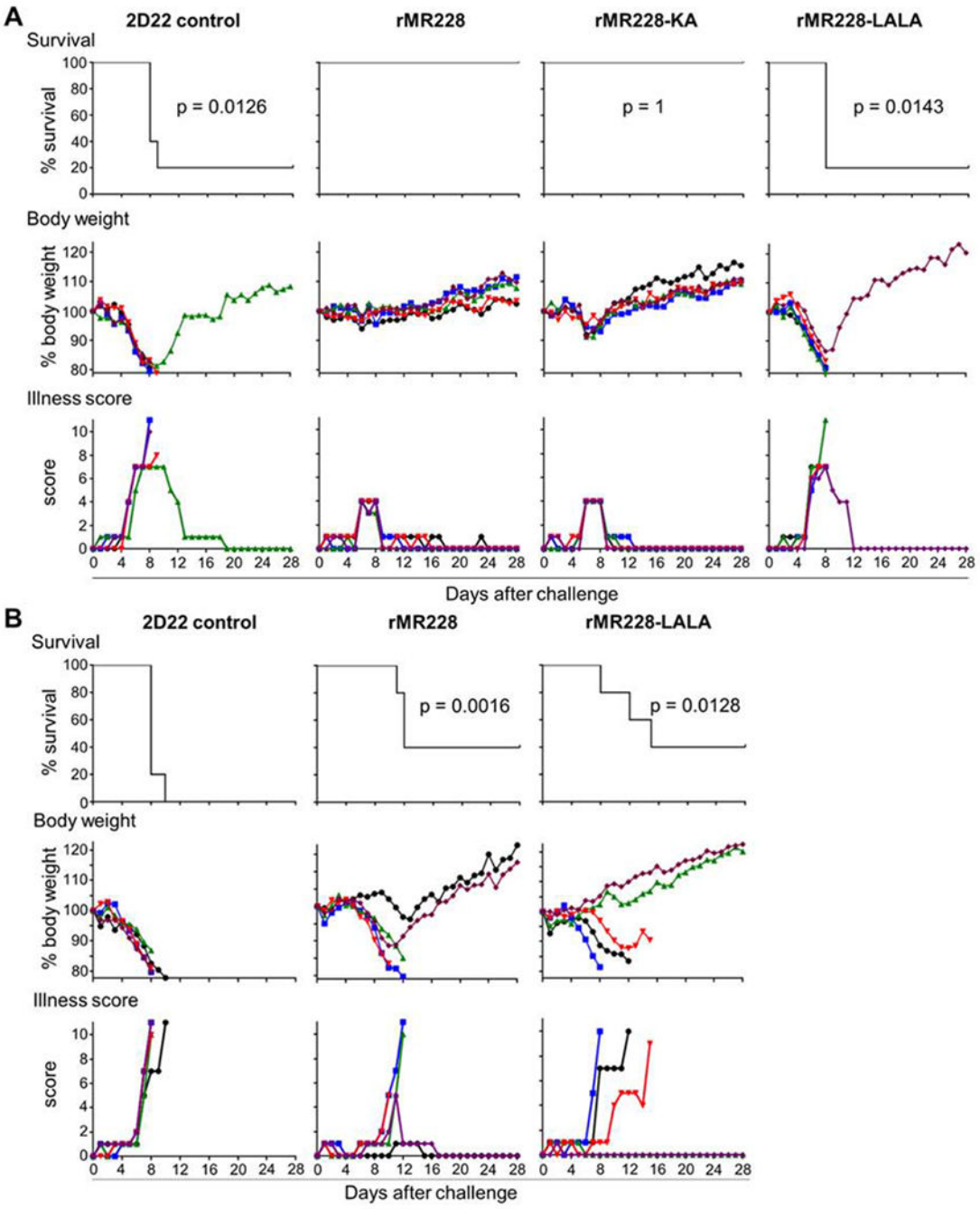

Fig. 4. MR228 protects against MARV infection *in vivo*.

Groups of mice **(A)** or guinea pigs **(B)** at five animals per group were injected with the indicated mAbs by the intraperitoneal route at 24 h after MARV challenge. Kaplan-Meier survival curves, body weight and illness score curves are shown. In (A) each group was compared to rMR228, and in (B) each group was compared to 2D22 control (Mantel-Cox test).

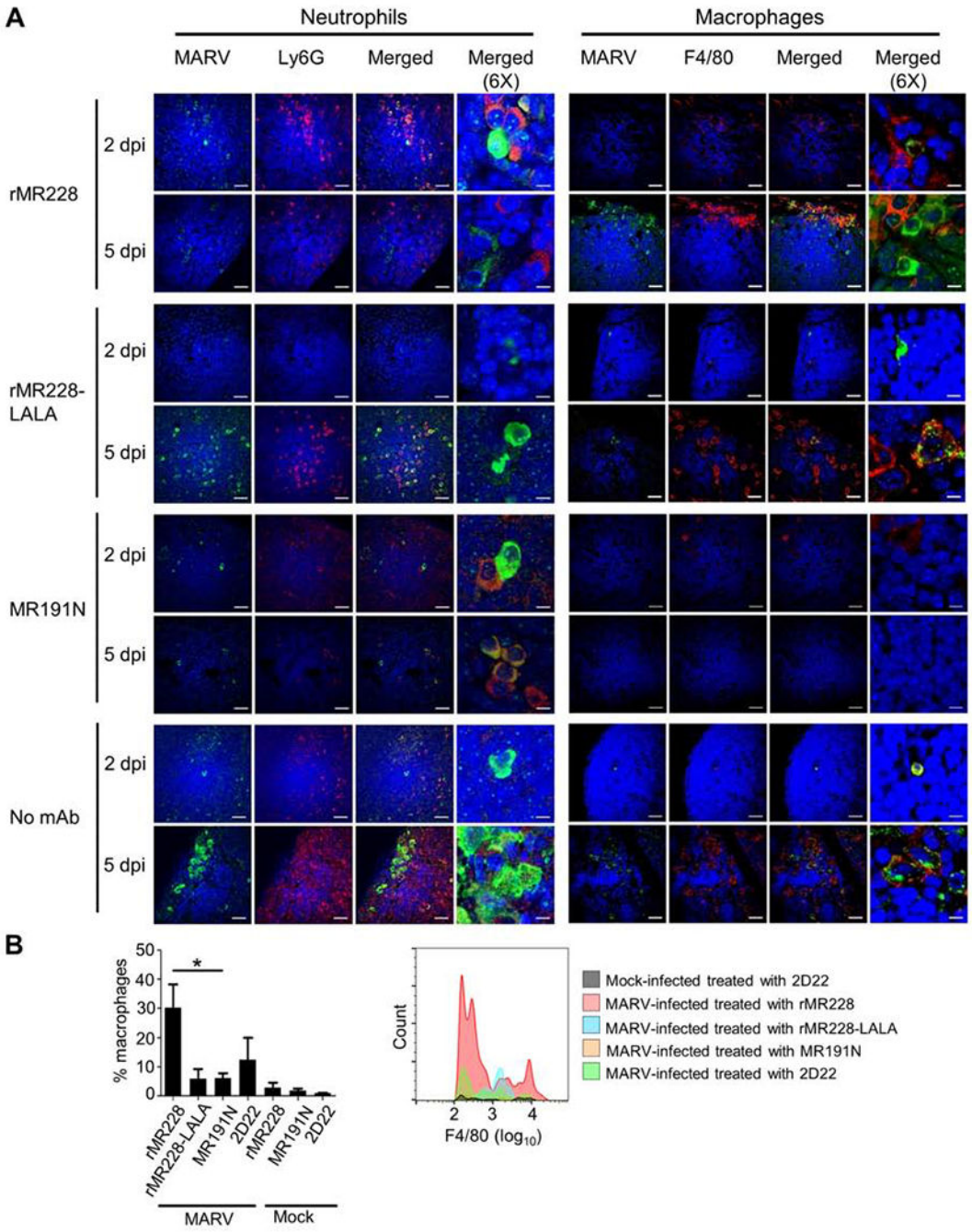

Fig. 5. Neutrophils and macrophages detected in lymph nodes of MARV-infected mice.

(A) Confocal microscopy. Green, MARV; red, Ly6G (for neutrophils, the left side) or F4/80 (for macrophages, right side). The scale bars correspond to 30 μm in the 1X images and 5 μm in the 6X zoom images. **(B)** Flow cytometric analysis of inflammatory influx of macrophages in mesenteric lymph nodes of infected (day 2 post infection) and uninfected mice. Left: macrophages (defined as $CD11b^{high}$, $F4/80^{high}$, $Ly6C^{+}$) as percentages of total CD11b-positive cells, mean values based on 3 (MARV-infected) or 2 (mock-infected) animals ± SEM. P values were calculated by unpaired Student's t test; * $p < 0.05$. Right:

representative primary flow cytometry data showing F4/80 expression in the $CD11b^{high}$, $F4/80^{high}$, $Ly6C^{+}$ population.

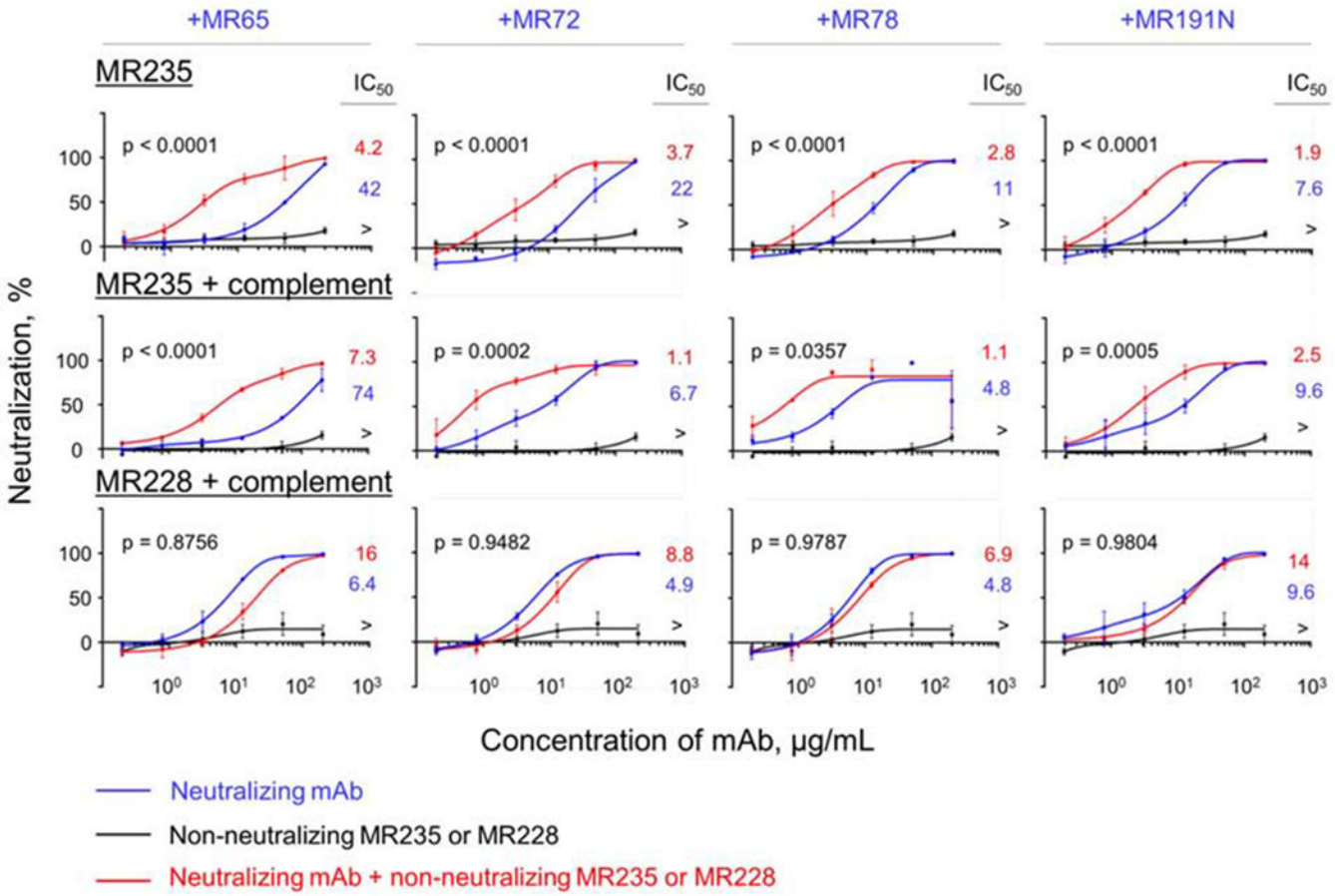

Fig. 6. MR235, but not MR228, enhances mAb-mediated virus neutralization *in vitro*.

Percent neutralization by the indicated mAbs or their combinations. The values on the X axes indicate concentration of individual mAbs or 1:1 combinations of two mAbs. At any given concentration, the total amount of combined mAbs was the same as that of the individual mAbs. Mean ± SD of technical triplicates are shown. Mean IC_{50} values µg/mL) for each mAb or combination are shown; > indicates neutralization was not detected at the highest concentration tested, 200 µg/mL. Each panel data were analyzed by One-Way ANOVA with Tukey's correction for multiple comparison testing; p values represent the comparison of IC_{50} (log_{10} µg/mL) for neutralizing mAb (blue curve) versus neutralizing + non-neutralizing mAb (red curve).

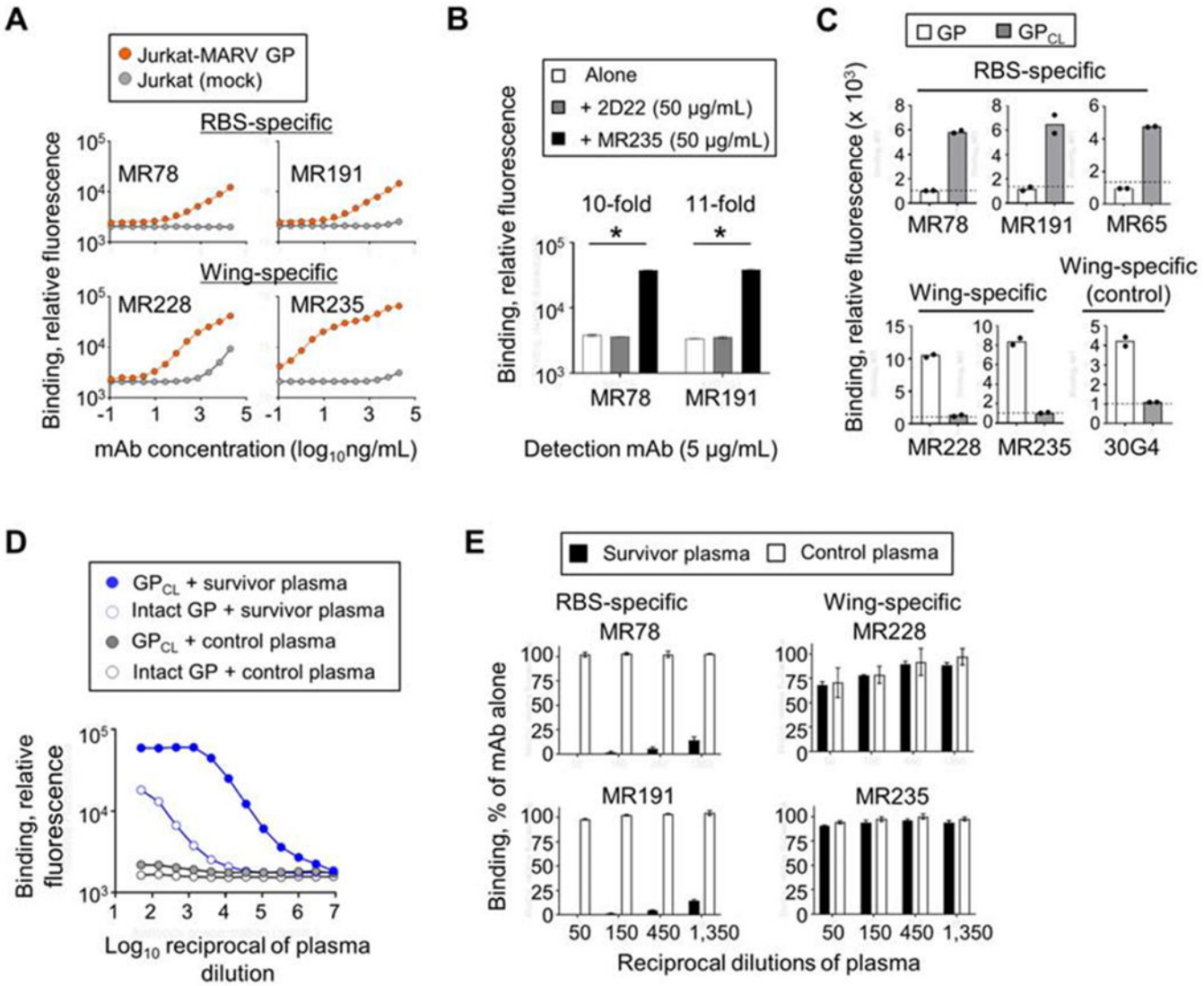

Fig. 7. MARV GP RBS is partially shielded, and non-neutralizing mAb MR235 potentiates binding of prevalent in plasma neutralizing mAbs to the GP.

(A) Binding of RBS- and wing-specific mAbs to cell surface displayed MARV GP. MAbs were incubated with Jurkat-MARV GP or mock Jurkat (control) cells at the indicated concentrations in triplicate, then incubated with secondary PE-labeled detection antibody, and binding was assessed by flow cytometric analysis. MFI ± SD of triplicate samples is shown. **(B)** MR235 facilitates binding of RBS-specific mAbs to Jurkat-MARV GP. MAbs MR78 or MR191 labeled with Alexa Fluor 647 fluorescent dye were titrated into fixed concentration (50 µg/mL) of unlabeled mAb MR235 or control mAb 2D22, then incubated with Jurkat-MARV GP or Jurkat mock cells (control for the background) and analyzed by flow cytometry. Background values (mean = 2,570 relative fluorescence units) were subtracted. Mean values ± SD of triplicate samples are shown; * $p < 0.0001$ (unpaired Student's t-test). **(C)** Jurkat-MARV GP cells were treated with thermolysin to generate cleaved GP (GP_{CL}) or left untreated. Cells were stained with respective mAbs, and binding was analyzed as in (A). Individual data points of technical duplicates and mean values (bars)

are shown. The dotted lines indicate the background from mAbs binding to control normal Jurkat cells. **(D)** Binding of Abs in plasma from the survivor or control donor to intact (intact GP) and cleaved (GP_{CL}) cell surface displayed MARV GP. Binding was assessed by flow cytometric analysis as in (A). Median fluorescence intensity ± SD of triplicate samples is shown. The error bars are not seen due to the very low sample-to-sample variation. **(E)** Competition-binding of plasma Abs with RBS- or wing-specific mAbs was assessed using cell surface displayed GP_{CL} and intact GP, respectively. Cells were pre-incubated with indicated dilutions of plasma from the survivor or control donor and then stained with respective mAbs. Background was determined from binding to mock Jurkat. Results are expressed as the percentage of mAb binding in the presence of plasma relative to mAb-only control (100% binding) minus background. Means ± SD of assay triplicates are shown.

KEY RESOURCES TABLE

REAGENT or RESOURCE	SOURCE	IDENTIFIER
Antibodies		
2D22	Fibriansah et al., 2015	N/A
30G4	Fusco et al., 2015	N/A
MR73	Flyak et al., 2015	N/A
MR114	Flyak et al., 2015	N/A
MR237	Flyak et al., 2015	N/A
MR228	Flyak et al., 2015	N/A
MR235	Flyak et al., 2015	N/A
MR162	Flyak et al., 2015	N/A
MR221	Flyak et al., 2015	N/A
MR246	Flyak et al., 2015	N/A
MR224	Flyak et al., 2015	N/A
MR65	Flyak et al., 2015	N/A
MR72	Flyak et al., 2015	N/A
MR78	Flyak et al., 2015	N/A
MR79	Flyak et al., 2015	N/A
MR82	Flyak et al., 2015	N/A
MR103	Flyak et al., 2015	N/A
MR111	Flyak et al., 2015	N/A
MR144	Flyak et al., 2015	N/A
MR186	Flyak et al., 2015	N/A
MR191	Flyak et al., 2015	N/A
MR198	Flyak et al., 2015	N/A
MR201	Flyak et al., 2015	N/A
MR208	Flyak et al., 2015	N/A
MR209	Flyak et al., 2015	N/A
MR213	Flyak et al., 2015	N/A
MR229	Flyak et al., 2015	N/A
MR232	Flyak et al., 2015	N/A
MR238	Flyak et al., 2015	N/A
MR241	Flyak et al., 2015	N/A
rMR228 (recombinant Expi293F-produced)	This paper	N/A
rMR228-LALA (recombinant Expi293F-produced)	This paper	N/A
rMR228-KA (recombinant Expi293F-produced)	This paper	N/A
MR186N (recombinant tobacco-produced)	This paper	N/A
MR191N (recombinant tobacco-produced)	This paper	N/A
Mouse anti-human IgG1 Hinge-AP	Southern Biotech	Cat#9052-04; RRID: AB_2687996

REAGENT or RESOURCE	SOURCE	IDENTIFIER
Mouse anti-human IgG2 Fc-AP	Southern Biotech	Cat#9070-04; RRID: AB_2687997
Mouse anti-human IgG3 Hinge-AP	Southern Biotech	Cat#9210-04; RRID: AB_2687998
Mouse anti-human IgG4 Fc-AP	Southern Biotech	Cat#9200-04; RRID: AB_2687999
Rat anti-mouse F4/80 (clone A3.1)	Abcam	Cat#Ab6640; RRID: AB_1140040
Rat anti-mouse Ly6G (clone 1A8)	MilliporeSigma	Cat#MABF839
Rat anti-mouse CD3 (clone CD3.12)	Abcam	Cat#Ab11089; RRID: AB_369097
Mouse anti-mouse NK1.1 (clone PK136)	MilliporeSigma	Cat#MABF1495Z
Rat anti-mouse Ly6C-PerCP-Cy5.5 (clone HK1.4)	BioLegend	Cat#128012; RRID: AB_1659241
Rat anti-mouse/human CD11b-BV421 (clone M1/70)	BioLegend	Cat#101236; RRID: AB_11203704
Rat anti-mouse F4/80-APC (clone BM8)	BioLegend	Cat#123116; RRID: AB_893481
Mouse anti-human CD66b-PE (clone G10F5)	BioLegend	Cat#305106; RRID: AB_2077857
Mouse anti-human CD3-AF700 (clone UCHT1)	BD Biosciences	Cat#557943; RRID: AB_396952
Mouse anti-human CD14-BV421 (Clone MφP9)	BD Biosciences	Cat#563743; RRID: AB_2744289
Mouse anti-human CD14-APC-Cy7 (Clone MφP9)	BD Biosciences	Cat#557831; RRID: AB_396889
Mouse anti-human CD14-PB (clone M5E2)	BioLegend	Cat#301828; RRID: AB_2275670
Mouse anti-human CD16-APC-Cy7 (Clone 3G8)	BD Biosciences	Cat#557758; RRID: AB_396864
Mouse anti-human CD107a-PE-Cy5 (Clone H4A3)	BD Biosciences	Cat#555802; RRID: AB_396136
Mouse anti-human IFNγ-APC (Clone B27)	BD Biosciences	Cat#554702; RRID: AB_398580
Mouse anti-human MIP-1β-PE (Clone D21-1351)	BD Biosciences	Cat#550078; RRID: AB_393549
Donkey anti-rat IgG(H+L)-Biotin	ThermoFisher Scientific	Cat#A18743; RRID: AB_2535520
Donkey anti-rabbit IgG(H+L)-AF488	ThermoFisher Scientific	Cat#A21206; RRID: AB_2535792
Goat anti-human IgG-PE	Southern Biotech	Cat#2040-09; RRID: AB_2795648
Goat anti-human IgG-HRP	Southern Biotech	Cat#2040-05; RRID: AB_2795644
Goat anti-human IgG(Fc)-HRP	Invitrogen	Cat#31413; RRID: AB_429693
Goat anti-human IgG(H+L)-AF488	Invitrogen	Cat#A-11013; RRID: AB_141360
Goat anti-human IgG(Fc)-AF647	Jackson ImmunoResearch Laboratories	Cat#109-605-098; RRID: AB_2337889
Goat anti-human IgG(H+L)-AF488	Jackson ImmunoResearch Laboratories	Cat#109-545-003; RRID: AB_2337831
Goat anti-rabbit IgG(H+L)-FITC	Southern Biotech	Cat#4050-02; RRID: AB_2795952
Rabbit anti-MARV GP, polyclonal	IBT Bioservices	Cat#0303-007; RRID: AB_2827726
Rabbit anti-MARV VLP, polyclonal	IBT Bioservices	Cat#04-0005; RRID: AB_2827760
Rabbit anti-MARV VLP serum	IBT Bioservices	Cat#01-0005; RRID: AB_2827761
Rabbit anti-MARV (Musoke) serum	T.G. Ksiazek	N/A
Bacterial and Virus Strains		
MARV strain 200501379 Angola (MARV-Angola)	Towner et al., 2006	N/A
The mouse-adapted Ci67 strain of MARV	Warfield et al., 2007	N/A
The guinea pig-adapted Angola strain of MARV	G. Kobinger	N/A
Chimeric EBOV/MARV-GP (GenBank: KU174140)	Ilinykh et al., 2016	N/A
VSV/MARV-GP	Flyak et al., 2015	N/A

REAGENT or RESOURCE	SOURCE	IDENTIFIER
Biological Samples		
MARV survivor plasma	Flyak et al., 2015	N/A
Plasma from a donor without an exposure history to filovirus infection	This paper	N/A
Chemicals, Peptides, and Recombinant Proteins		
Tragacanth	Spectrum Chemical	Cat#TR105
4′,6-diamidino-2-phenylindole (DAPI)	ThermoFisher Scientific	Cat#D1306
Sudan Black	Sigma-Aldrich	Cat#199664
CellTrace-FarRed	ThermoFisher Scientific	Cat#C34564
Alexa Fluor 647 NHS ester	ThermoFisher Scientific	Cat#A37573
Streptavidin conjugated with Alexa Fluor 647	ThermoFisher Scientific	Cat#S32357
1-Step Ultra TMB-ELISA	ThermoFisher Scientific	Cat#34029
ECL substrate	ThermoFisher Scientific	Cat#34580
Cellstripper	Cellgro	Cat#25-056-CI
DAKO Target Retrieval Solution	Dako North America Inc.	Cat#S1699
JPT washing buffer	JPT Peptide Technologies GmbH	Cat#RT_Kit_01
BD Stain Buffer (FBS)	BD Biosciences	Cat#554656
BD Cytofix/Cytoperm	BD Biosciences	Cat#554722
Fix/Perm	Life Technologies	Cat # GAS001S100 and GAS002S-100
Brefeldin A	MilliporeSigma	Cat#B7651
GolgiStop	Life Technologies	Cat#554724
Thermolysin	Promega	Cat#9PIV400
Ethylenediaminetetraacetic acid (EDTA)	Sigma-Aldrich	Cat#E5134
NuPAGE LDS Sample Buffer	ThermoFisher Scientific	Cat#NP0007
Dithiothreitol (DTT)	ThermoFisher Scientific	Cat#R0861
Sodium azide	Sigma-Aldrich	Cat#13412
TRIzol reagent	ThermoFisher Scientific	Cat#15596018
Phosphate-buffered formalin	ThermoFisher Scientific	Cat#245-684
16% formaldehyde, methanol-free	Polysciences	Cat#18814-10
Tween-20	Sigma-Aldrich	Cat#P9416-100ML
Triton X-100	Sigma-Aldrich	Cat#T8787-100ML
Freestyle 293 Expression Medium	ThermoFisher Scientific	Cat#12338002
ExpiCHO Expression Medium	ThermoFisher Scientific	Cat#A2910001
RPMI 1640 Medium	Sigma-Aldrich	Cat#R0883
Minimal Essential Medium	ThermoFisher Scientific	Cat#11095-080
High glucose Dulbecco’s Minimal Essential Medium	ThermoFisher Scientific	Cat#11965092
Fetal Bovine Serum	HyClone	Cat#SH30910.03HI-ST
Fetal Bovine Serum	Sigma-Aldrich	Cat#F4135
Fetal Bovine Serum, ultra-low IgG	ThermoFisher Scientific	Cat#16250078

REAGENT or RESOURCE	SOURCE	IDENTIFIER
Streptomycin	Gibco	Cat#15070-063
Penicillin-streptomycin	Invitrogen	Cat#15140122
Beta-mercaptoethanol	Gibco	Cat#21985023
Bovine serum albumin	MilliporeSigma	Cat#820451
Dulbecco's phosphate-buffered saline	Corning	Cat#21-031-CV
Guinea pig complement	MP Biomedicals	Cat#642836
Normal goat serum	ThermoFisher Scientific	Cat#16210072
Non-immune rabbit serum	MilliporeSigma	Cat#R9133
Overlapping 15-mer peptides corresponding to MARV strain 200501379 Angola GP sequence	JPT Peptide Technologies GmbH	N/A
Musoke GP ectodomain	Fusco et al., 2015; Hashiguchi et al., 2015	N/A
Angola GP ectodomain	Fusco et al., 2015; Hashiguchi et al., 2015	N/A
Popp GP ectodomain	Fusco et al., 2015; Hashiguchi et al., 2015	N/A
RAVV GP ectodomain	Fusco et al., 2015; Hashiguchi et al., 2015	N/A
Musoke GPΔmuc ectodomain	Fusco et al., 2015; Hashiguchi et al., 2015	N/A
Angola GPΔmuc ectodomain	Fusco et al., 2015; Hashiguchi et al., 2015	N/A
RAVV GPΔmuc ectodomain	Fusco et al., 2015; Hashiguchi et al., 2015	N/A
MARV GP ΔTM (aa 1-648; Angola 2005)	This paper	N/A
Biotinylated recombinant MARV GP protein (strain Angola)	IBT Bioservices	Cat#0506-015
Critical Commercial Assays		
EasySep human monocyte enrichment kit	StemCell	Cat#19058
Live/Dead Fixable Dead Cell Stain kit, Acqua	ThermoFisher Scientific	Cat#L34957
Mouse-On-Mouse kit	Vector labs	Cat#BMK2202; RRID: AB_2336833
4CN two-component peroxidase substrate system	KPL	Cat#5420-0024
Q5 Site-Directed Mutagenesis Kit	New England BioLabs	Cat#E0554S
T4 quick ligation kit	New England BioLabs	Cat#M2200S
PrimeScript One Step RT-PCR kit	Clontech	Cat#RR055B
RNeasy Mini kit	Qiagen	Cat#74104
Deposited Data		
Peptide microarray	This paper; Mendeley Data	Fig. 3B,C; https://data.mendeley.com/datasets/yrhzkttr73/1
Epitope mapping using a MARV GP alanine-scan mutation library	This paper; Mendeley Data	Fig. S4C; https://data.mendeley.com/datasets/b8ckvvdmr6/1
Experimental Models: Cell Lines		
Human: Expi293F	ThermoFisher Scientific	Cat#A14528; RRID: CVCL_D615

REAGENT or RESOURCE	SOURCE	IDENTIFIER
Human: FreeStyle 293-F	ThermoFisher Scientific	Cat#R79007; RRID: CVCL_D603
Human: HEK-293T	ATCC	Cat#CRL-3216; RRID:CVCL_0063
Human: THP-1	ATCC	Cat#TIB-202; RRID:CVCL_0006
Human: Jurkat, clone E6-1	ATCC	Cat#TIB-152; RRID: CVCL_0367
Human: Jurkat-MARV GP (Angola)	C.W. Davis and R. Ahmed	N/A
Monkey: Vero-E6	ATCC	ATCC: CRL-1586
Hamster: ExpiCHO-S	ThermoFisher Scientific	Cat#A29127; RRID: CVCL_5J31
Experimental Models: Organisms/Strains		
Mouse: BALB/cJ	The Jackson Laboratory	Cat#JAX:000651; RRID: IMSR_JAX:000651
Guinea pig: Hartley	Charles River Laboratories	Cat#051; RRID: NCBITaxon_10141
Oligonucleotides		
Recombinant DNA		
pCAGGS MCSII mammalian vector expressing wild-type MARV Musoke strain GP	C.F. Basler	N/A
pMARVGP(450GLIN453 → AAAA)	This paper	N/A
pMARVGP(461VPNTK466 → AAAAA)	This paper	N/A
pMARVGP(D449A/N453A/D457A/D459A)	This paper	N/A
pMARVGP(T545A/E634A/G635A)	This paper	N/A
pMARVGP(P455A)	This paper	N/A
pMARVGP(R597A)	This paper	N/A
pMARVGP(W598A)	This paper	N/A
pMARVGP(T601A)	This paper	N/A
pMARVGP(K603A)	This paper	N/A
pMARVGP(L605A)	This paper	N/A
pMARVGP(P607A)	This paper	N/A
pMARVGP(D608A)	This paper	N/A
pMARVGP(Del 411-430aa)	This paper	N/A
pMARVGP(Del 237-425aa)	This paper	N/A
pMARVGP(Del 411-442aa)	This paper	N/A
pMARVGP(Del 436-500aa)	This paper	N/A
pMARVGP(Del 441-459aa)	This paper	N/A
pCMV Marburgvirus-GP[Δmucin] [01Uga2007]	This paper	N/A
Software and Algorithms		
GraphPad Prism 7.2	GraphPad Software, Inc.	GraphPad Prism; RRID: SCR_002798
GraphPad Prism 6.05	GraphPad Software, Inc.	GraphPad Prism
FlowJo version 10	Tree Star Inc.	FlowJo; RRID: SCR_008520
FlowJo software, version 7.6.1	FlowJo LLC	FlowJo; RRID: SCR_008520

REAGENT or RESOURCE	SOURCE	IDENTIFIER
ForeCyt Standard 6.2 (R1)	Intellicyt	ForeCyt
GenePix Pro 6	Molecular Devices	N/A
Interpretation of shotgun mutagenesis data, custom in-house software	Davidson and Doranz, 2014	N/A
BioEdit 7.2.5	http://www.mbio.ncsu.edu/BioEdit/bioedit.html	BioEdit; RRID:SCR_007361
UCSF Chimera	www.cgl.ucsf.edu/chimera	N/A
Other		
ABI3700 automated DNA analyzer	Applied Biosystems	N/A
FACSCanto II instrument	BD Biosciences	N/A
LSRII flow cytometer	BD Biosciences	3 laser model
Intellicyt iQue high throughput flow cytometer	Sartorius	iQue3
Accuri C6 Plus cytometer	BD Biosciences	Cat#660517-BD
ÄKTA pure chromatography system	GE Healthcare Life Sciences	N/A
GenePix 4000b	Molecular Devices	N/A
Olympus FV1000 confocal microscope	Olympus	N/A
2104 EnVision multilabel reader	Perkin-Elmer	Cat#2104-0010
Synergy H1 microplate reader	BioTek	N/A
EL406 washer dispenser	BioTek	N/A
Biostack microplate stacker	BioTek	N/A
HiTrap Protein G High Performance	GE Healthcare Life Sciences	Cat#28-9075-48
HiTrap MabSelect™ SuRe 5 mL column	GE Healthcare Life Sciences	Cat#17-0404-01
Superdex 200 Increase 10/300 GL column	GE Healthcare Life Sciences	Cat#PI-89883
Zeba™ Spin Desalting Columns	ThermoFisher Scientific	Cat#89882
StrepTrap HP	GE Healthcare Life Sciences	N/A
Agencourt AMPure XP magnetic beads	Beckman Coulter	CAT (Pavlo)
Yellow-green Neutravidin beads	Life Technologies	Cat#F-8776
SDS-PAGE gels	Bio-Rad	Cat#456-8086
Polyvinylidene difluoride membranes	MilliporeSigma	Cat#IPVH07850